communications biology

A Nature Portfolio journal

Article

https://doi.org/10.1038/s42003-025-08284-5

Costs of photosynthesis and cellular remodeling in trophic transitions of the unicellular red alga *Galdieria partita*

Shota Yamashita [1] ✉, Shunsuke Hirooka [1], Takayuki Fujiwara [1,2], Baifeng Zhou [1], Fumi Yagisawa [3], Kei Tamashiro[4], Hiroki Murakami [5], Koichiro Awai [6] & Shin-ya Miyagishima [1,2] ✉

As in plastid differentiation in land plants, some unicellular algae reversibly remodel photosynthetic plastids into a colorless heterotrophic state (bleaching) in the presence of organic carbon sources. To understand these mechanisms and their significance, we performed comparative omics analyses on the photoautotrophic and heterotrophic states and their transitions in the genetically tractable red alga *Galdieria partita*. Photoautotrophic cells require 1.5, 1.3 and 1.7 times more nitrogen, protein, and fatty acids than heterotrophic cells. In the photoautotrophic cells, plastid- and nucleus-encoded proteins for photosynthesis are highly synthesized, while in the heterotrophic state, cytoplasmic and mitochondrial proteins are more abundant, enabling 1.6 times faster growth. Changes in non-plastid metabolic enzymes are limited, with some upregulated in the photoautotrophic state to support fatty acid and glycolipid synthesis in the plastid for thylakoid membranes. In contrast, solute transporters show broader changes. Bleaching occurs upon adding certain sugars or sugar alcohols, regardless of light, not by active digestion of photosynthetic machinery, but by dilution due to suppressed synthesis at the transcriptional level and faster cell growth. Thus, when assimilable organic carbon is available, the cells repress the synthesis of proteins, lipids, and pigments for photosynthesis, reallocating resources to promote faster growth.

Photosynthetic organisms have originated and evolved across various eukaryotic lineages through the integration of cyanobacterial or algal cells. The common ancestor of Archaeplastida which includes red algae, glaucophytes, green algae, and land plants, genetically integrated a cyanobacterial endosymbiont into a primary plastid as a photosynthetic organelle more than one billion years ago. Another photosynthetic organelle, the chromatophore, was more recently established in cercozoan *Paulinella* through the integration of a cyanobacterium. Many other eukaryotic lineages, such as stramenopiles, plastid-bearing alveolates, haptophytes, cryptophytes, euglenids, and chlorarachniophytes, acquired plastids through secondary endosymbiotic events involving a unicellular red or green alga, or even through higher-order endosymbiosis, such as the integration of an alga with a secondary plastid[1–4].

The ancestors of these photosynthetic eukaryotes were heterotrophs that likely first became mixotrophic organisms by integrating cyanobacteria or algae as plastids. Many photosynthetic eukaryotes retain this mixotrophic capacity, combining photosynthesis with phagotrophy or osmotrophy (absorbing dissolved organic substrates), and they occupy a large portion of terrestrial and aquatic ecosystems[5–7]. Furthermore, some organisms are facultative mixotrophs, capable of growing through heterotrophy, photoautotrophy, or mixotrophy, by any means (e.g., the diatom *Navicula saprophila*[8] and the chrysophyte *Ochromonas*[9]). Thus, it is believed that obligate photoautotrophs emerged by losing their capability for heterotrophic growth (i.e., capability of growing in the dark), while in some cases, mixotrophic ancestors secondarily lost their photosynthetic abilities and reverted to heterotrophs[6].

Land plants, which evolved from a green algal ancestor, the major primary producers in terrestrial ecosystems, are also mixotrophic. While some lineages have evolved obvious mixotrophic or even heterotrophic strategies, such as carnivory, hemiparasitism, and mycoheterotrophy, many other lineages in land plants also have the ability to absorb external organic carbon sources through their roots[6,10,11]. In addition, land plants have

[1]Department of Gene Function and Phenomics, National Institute of Genetics, Shizuoka, Japan. [2]Genetics Program, Graduate University for Advanced Studies (SOKENDAI), Shizuoka, Japan. [3]Research Facility Center, University of the Ryukyus, Okinawa, Japan. [4]Integrated Technology Center, University of the Ryukyus, Okinawa, Japan. [5]Faculty of Global Interdisciplinary Science and Innovation, Shizuoka University, Shizuoka, Japan. [6]Faculty of Science, Shizuoka University, Shizuoka, Japan. ✉e-mail: yamashii@nig.ac.jp; smiyagis@nig.ac.jp

developed complex multicellular organization that involves the differentiation of phototrophic and heterotrophic cells, tissues, and organs, such as photosynthetic leaves and heterotrophic roots, within an individual body. The cells in heterotrophic tissues possess non-photosynthetic plastids, such as proplastids, amyloplasts, or chromoplasts, depending on the functions of the tissues, while the cells in phototrophic tissues possess photosynthetic plastids, the chloroplasts[12]. It is believed that the mechanisms of cellular differentiation, involving the differentiation of plastids, emerged after land plants evolved a complex multicellular lifestyle[12,13].

However, it is also known that some unicellular mixotrophic algae are capable of largely remodeling their intracellular composition, including plastids, in response to the availability of assimilable organic compounds in the environment. As prime examples, the plastids reversibly lose their photosynthetic pigments thus photosynthetic activity (bleaching) upon the addition of glucose to inorganic culture media in the green algae *Auxenochlorella protothecoides*[14] and *Chromochloris zofingiensis*[15], as well as in the red algae *Galdieria* spp[16,17]. In addition, *A. protothecoides* cells accumulate lipids outside the plastid[18], and *C. zofingiensis* cells accumulate astaxanthin in addition to lipids, both inside and outside the plastid[15,19,20] under mixotrophic (with glucose in the light) and heterotrophic (with glucose in the dark) conditions. The green alga *Chlamydomonas reinhardtii*, a model unicellular alga, is a facultative mixotroph that can assimilate acetate as a carbon source and exhibits reduced photosynthetic activity when acetate is added to the culture, though the plastid retains its green color[21–23]. These features of extant algal species raise the possibility that the unicellular common ancestors of plants and algae already possessed a mechanism to remodel cells into a photoautotrophic state with a photosynthetic plastid and a heterotrophic state with a non-photosynthetic plastid. Such a system may have been later co-opted for cellular differentiation in multicellular land plants. Alternatively, the unicellular ancestors of photosynthetic eukaryotes may have possessed the potential to independently evolve a mechanism for cellular remodeling involving plastid differentiation.

One possible advantage of abandoning photosynthetic ability when an organism can grow heterotrophically is the reduction in energy and resource costs associated with photosynthesis. To perform photosynthesis, the plastid needs to be equipped with numerous photosynthetic machineries consisting of protein complexes embedded in the thylakoid membranes, which convert absorbed light energy into reducing power and ATP. Additionally, it requires many enzymes involved in carbon fixation to generate carbohydrates using the reducing power and ATP, such as ribulose-1,5-bisphosphate carboxylase/oxygenase (Rubisco), which is the most abundant enzyme in photosynthetic cells[24,25]. Previously, it was estimated in phototrophic algae that 50% of the cellular resources are devoted to the photosynthetic apparatus[26], while another study in plant leaves estimated that 54% of the total nitrogen is allocated to synthesize amino acids, proteins, nucleic acids, and other components for photosynthesis[27]. However, there has been no study that has measured the exact cost of performing photosynthesis by comparing the photoautotrophic and heterotrophic states within a single unicellular organism.

Regarding cellular remodeling, transcriptome analyses of the bleaching and greening processes have been conducted in the green alga *C. zofingiensis*[15]. Additionally, comparative transcriptome analyses of the photoautotrophic and heterotrophic states have been performed in the red alga *G. javensis* 074W[28] (reclassified from *G. sulphuraria* 074W[29]), and proteomic and metabolomic analyses of *G. sulphuraria* SAG21.92, cultivated in photoautotrophic, mixotrophic, and heterotrophic states, were conducted[30], advancing our understanding of the differences between trophic states. For example, in *C. zofingiensis*, the addition of glucose to the culture downregulated photosynthetic genes, while ketocarotenoid biosynthesis, glycolysis, and fatty acid biosynthesis were upregulated[15]. In the heterotrophic state in *G. javensis*, acetate, amino acid, and sugar transporters were downregulated as well as photosynthesis-related genes[28]. In mixotrophic growth in *G. sulphuraria* SAG21.92, CO_2 generated by enhanced respiration promoted photosynthesis and suppressed photorespiration[30]. However, the overall picture of how the cells are remodeled between photoautotrophic and heterotrophic states, as well as the precise cost of photosynthesis, remains unclear. In addition, the mechanism of remodeling is also poorly understood. These issues are largely due to the lack of genetically tractable model organisms among facultative mixotrophic algae that drastically change their intracellular composition, including plastid bleaching and greening.

The unicellular red alga *G. partita*, belonging to Cyanidiophyceae, would be a suitable model for investigating the cost of photosynthesis and the mechanism of cellular remodeling between the photoautotrophic and heterotrophic states. The class Cyanidiophyceae, consisting of four orders[29], is the most early-branching group within Rhodophyta (red algae). Algae in this class exhibit a blue-green color due to the lack of the red photosynthetic pigment phycoerythrin, and many of its species inhabit volcanic areas with sulfuric hot springs that have high temperatures (38–56°C) and low pH (0.2–4)[31–33]. While other orders in Cyanidiophyceae, including the genetically tractable model species *Cyanidioschyzon merolae*, are obligate photoautotrophs, the order Galdieriales (consisting of one genus, *Galdieria*) is facultative mixotrophic and can assimilate more than 50 different organic carbon sources, such as sugars, sugar alcohols, and amino acids[16,34–36]. In Galdieriales, the addition of sugars or sugar alcohols causes bleaching and a loss of photosynthetic activity[37] through a reduction in plastid size and thylakoid membranes[17,38], as well as chlorophyll *a* and phycocyanin[16,17]. The ancestors of red algae are assumed to have been mixotrophs, and the ability for heterotrophic growth have been retained in the order Galdieriales but lost in the common ancestor of the other three orders of Cyanidiophyceae. However, the capacity of Galdieriales to take up and utilize external carbon sources may have been further enhanced by genes acquired through horizontal gene transfer[39,40]. The nuclear, plastid, and mitochondrial genome sequences of *G. partita* were determined[41], and the size of the nuclear genome is relatively small among eukaryotic phototrophs (17.8 Mb with 7832 protein-coding genes), as in other cyanidiophycean species[39,40,42–45]. In addition, procedures for genetic modification have recently been developed in *G. partita*[41] by applying a polyethylene glycol (PEG)–mediated method, previously developed in *C. merolae*[46,47], to cell-wall-less haploid cells[41]. Together with the relatively simple intracellular architecture, the small genome and the procedures for genetic modification would facilitate elucidation of the mechanism underlying the remodeling of the photosynthetic and bleached heterotrophic states. In addition, Rhodophyta (red algae) and Viridiplantae (green algae and land plants), which form the two major lineages of Archaeplastida, branched approximately 1.5 billion years ago[48,49], relatively soon after plastids were established through cyanobacterial endosymbiosis. Rhodophyta also evolved multicellular lifestyles and heterotrophic tissues (carposporophytes) independently of land plants[50]. Thus, comparing the findings from studies in *G. partita* with those in green algae and land plants can provide deeper insights into the evolutionary processes underlying trophic modes and cellular remodeling.

Here, as a first step in the elucidation of the mechanism of cellular remodeling between the photoautotrophic and heterotrophic states, we compared various aspects of *G. partita* cells in the two trophic states in terms of intracellular composition, levels of organellar DNA and RNA, transcriptome, proteome, and metabolome. We estimated the cost of photosynthesis from these comparisons and identified the pathways that change between the two trophic states. In addition, we analyzed the course of transition between the photoautotrophic and heterotrophic states (bleaching and greening). The results suggest that the cells reduce the cost of photosynthesis by primarily altering specific pathways, such as the synthesis of photosynthetic apparatus, lipid synthesis, and solute transporters, in response to the availability of external organic carbon sources, and invest the saved resources in cell growth.

Results

Response of *G. partita* strain used in this study to the presence or absence of glucose

As far as has been investigated, any strain of the order Galdieriales is capable of reversible bleaching when supplied with exogenous glucose, although the

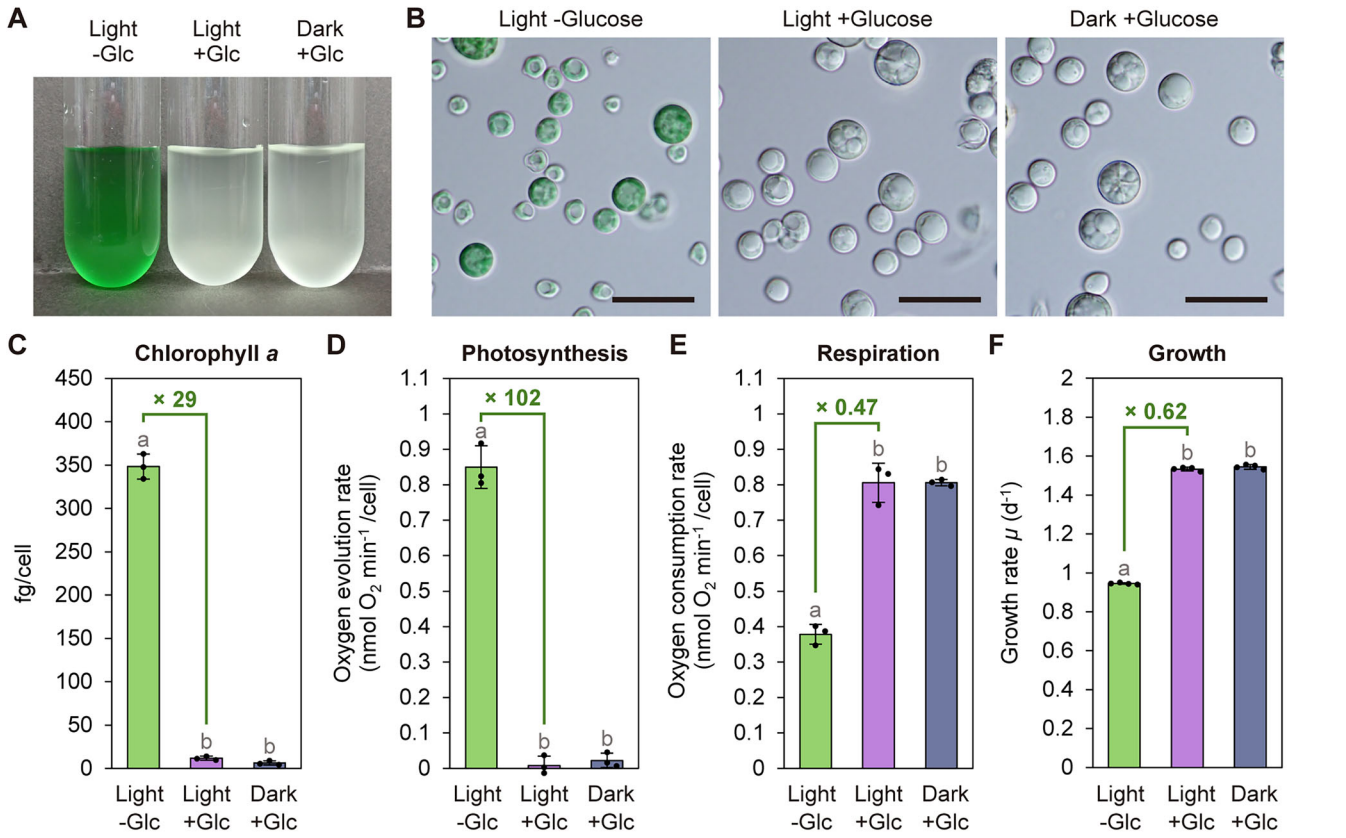

Fig. 1 | Characteristics of *G. partita* cells grown under the presence/absence of light and exogenous glucose. A Liquid culture of the wild-type *G. partita* diploid N2 grown in the light (50 μmol photon m^{-2} s^{-1}) or dark with or without 100 mM glucose (Glc) in the medium. The cells were repeatedly grown in batch cultures to obtain log-phase cultures steadily adapted to their respective culture conditions. **B** Micrographs of *G. partita* cells grown under the three different conditions. Scale bars = 20 μm. **C** Chlorophyll *a* content per cell grown under the three different conditions. **D** Net photosynthetic activity (oxygen evolution rate in the light at 100 μmol photons m^{-2} s^{-1}), and **E** respiratory activity (oxygen consumption rate in the dark) per cell grown under the three different conditions. Net photosynthesis was calculated as gross photosynthesis +|respiration|, assuming that oxygen consumption by respiration in the light is identical to that in the dark. **F** Growth rate of the cells measured during the logarithmic phase under the three different conditions. Bars represent means ± standard deviations (SD) of results from three (**C**–**E**) or four (**F**) independent cultures, with dots representing individual data points. Bars with the different letters (a versus b) are significantly different, while bars with the same letters (b versus b) are not, based on Tukey's honestly significant difference test at $P < 0.05$. The ratio of values in the light without glucose (the photoautotrophic state) to those in the light with glucose (the heterotrophic state) is shown above the bars.

extent of bleaching varies by strains. For example, *G. javensis* 074 W bleaches almost completely, whereas *G. sulphuraria* 074 G and SAG21.92 do not bleach entirely[16,30,39]. *G. partita* NBRC 102759, for which a procedure for genetic modification was recently developed, also bleaches to some extent in the presence of glucose, but not completely[41]. To efficiently compare the intracellular composition and metabolism between the photoautotrophic (green) and heterotrophic (bleached) states, as well as to evaluate the costs required for photosynthesis, we first selected and prepared a clone of *G. partita* that bleaches almost completely, as described below.

The naturally occurring cell-walled forms of Galdieriales are heterozygous diploids and have been cultured in laboratories at around pH 2.0, which produce cell-wall-less haploids in cultures at pH 1.0[41]. In our previous study, five haploid clones (N1 to N5) were generated from the original heterozygous diploid clone of *G. partita* NBRC 102759[41]. When these five haploid clones, along with an additional haploid clone (N6), were cultured on a glucose-supplemented plate medium in the dark, they exhibited varying degrees of bleaching: clones N2, N3, and N4 almost completely bleached, whereas clones N1, N5, and N6 did not (Supplementary Fig. 1A). Based on the result, we generated a homozygous diploid clone from the haploid clone N2 (hereafter referred to as *G. partita* diploid N2) by self-diploidization (spontaneous endoreduplication[41]). Based on the previously generated six haploid clones alone, the phenotypes appeared to segregate in a 1:1 ratio between completely bleached and non-bleached types. However, when we re-isolated a haploid population derived from the same original diploid clone, the cells exhibited a broad range of phenotypes—from green and pale green to bleached—with various colony sizes independent of coloration on a glucose-supplemented plate medium in the dark (Supplementary Fig. 1B). Thus, the bleaching phenotype and the heterotrophic growth rate are unlikely to be determined by a single genomic locus, but are more likely governed by multiple genes.

When *G. partita* diploid N2 was cultivated in the presence of exogenous glucose, and the cells were fully adapted to the respective culture conditions through several rounds of batch culture, they almost completely bleached, regardless of light or dark conditions (Fig. 1A, B; log-phase cultures were compared in Fig. 1). In the bleached cells, chlorophyll *a* (Fig. 1C) content and photosynthetic oxygen evolution (Fig. 1D) were almost completely lost, regardless of light availability. Thus, *G. partita* diploid N2 grows heterotrophically but not mixotrophically in the presence of exogenous glucose, even when light is available. This phenotype is similar to that of *G. sulphuraria* strain 074G[37] but different from that of *G. sulphuraria* SAG21.92, which grows mixotrophically by retaining photosynthetic activity in the presence of exogenous glucose and light[30]. In contrast to its photosynthetic activity, the heterotrophic state of *G. partita* diploid N2 in the light or dark exhibited approximately twice as much respiratory activity as the photoautotrophic state grown in an inorganic medium in the light (Fig. 1E). The growth rate in the heterotrophic state, in light or dark with no significant difference between them, was also 1.6 times higher than in the photoautotrophic state (Fig. 1F). These results suggest that *G. partita* diploid

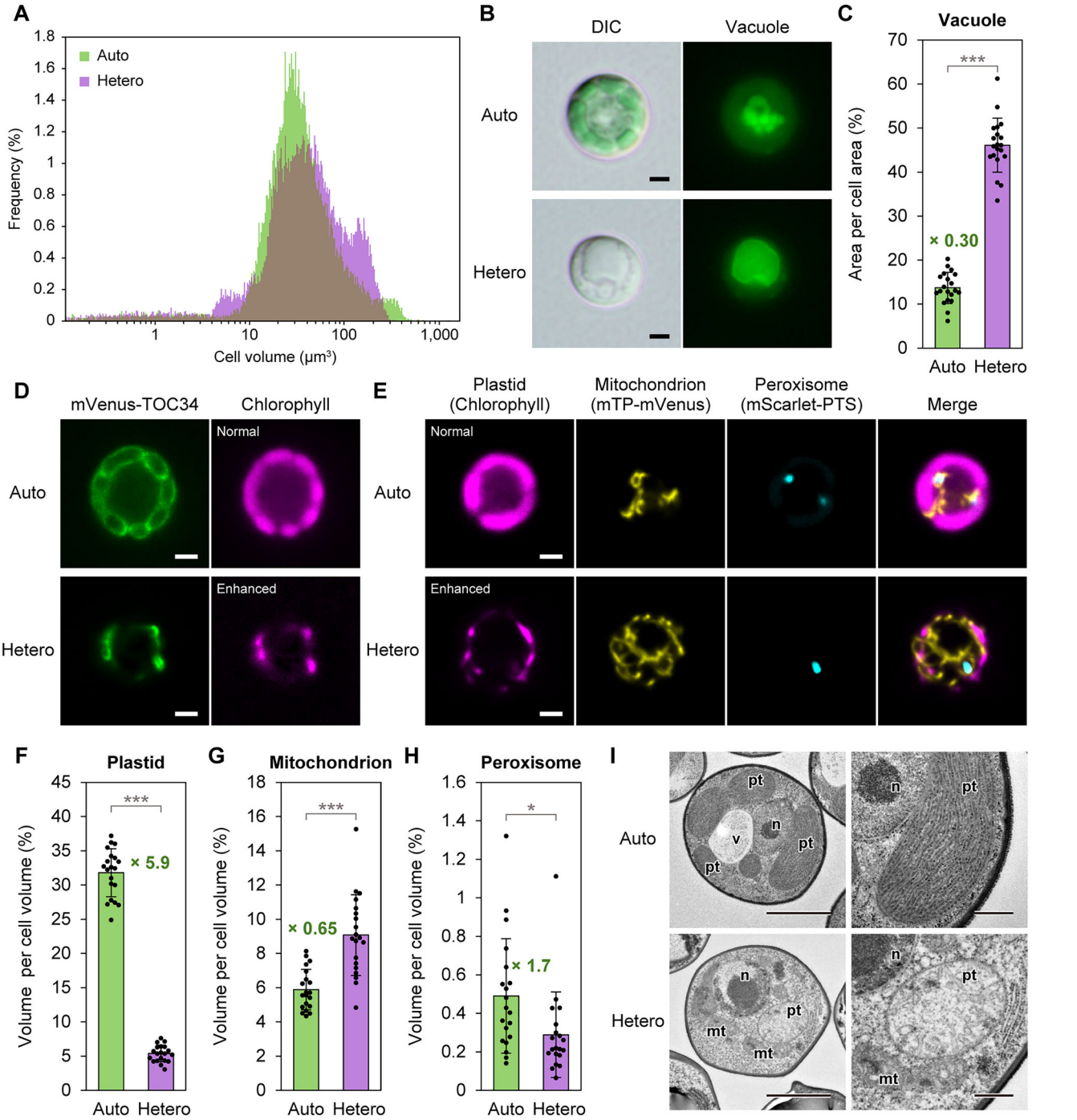

N2 cells are remodeled to an almost identical heterotrophic state in the presence of exogenous glucose, regardless of light availability. Thus, hereafter we compared cells in the photoautotrophic (green) and heterotrophic (bleached) states using log-phase cultures of *G. partita* diploid N2 (hereafter *G. partita*), fully adapted to the absence or presence of exogenous glucose, respectively, under light conditions.

Comparison of cellular and subcellular morphology in *G. partita* between the photoautotrophic and heterotrophic states

The distribution of cell size was nearly identical between the photoautotrophic and heterotrophic states (Fig. 2A). In the photoautotrophic cells, green plastids formed a thick layer just beneath the cell membrane, which were later found to be connected as a single organelle (Fig. 2B). In contrast, no green plastids were observed in the heterotrophic cells. Instead, in the heterotrophic state, a large vacuole was observed at the center of the cell with quinacrine staining (Fig. 2B), which was larger than that in the photoautotrophic state (Fig. 2C). As the quinacrine fluorescence rapidly decreased during excitation, three-dimensional (3D) images could not be obtained. Thus, images of the median optical section of the cells were compared (Fig. 2B, C).

To observe the colorless plastid in the heterotrophic cell, a transformant of *G. partita* expressing a fluorescent protein-tagged plastid outer membrane protein, mVenus-TOC34, was generated and observed by 3D fluorescence microscopy (Fig. 2D and Supplementary Movies 1 and 2). The thin, string-like shaped plastid was visualized in the heterotrophic state (Fig. 2D and Supplementary Movie 2). However, the morphology of the plastid was complex, making it difficult to quantify the volume of the region enclosed by the mVenus-TOC34 fluorescence. Nonetheless, when the

Fig. 2 | Comparison of the cellular and intracellular morphology of *G. partita* between the photoautotrophic and heterotrophic states. All results are from the photoautotrophic (in the light without glucose) and heterotrophic (in the light with glucose) cultures of wild-type diploid N2 and its derivatives. **A** Distribution of cell volume in the photoautotrophic and heterotrophic cultures of wild-type diploid N2. **B** Comparison of morphology of vacuoles between the photoautotrophic and heterotrophic cells (wild-type diploid N2). Differential interference contrast (DIC) images and fluorescence images of vacuoles stained with quinacrine dihydrochloride of the same cells are shown. Scale bars = 2 μm. **C** Percentage of vacuole area per cell area in the median optical section. Means ± SD of results from 20 independent cells are shown, with dots representing data points from individual cells. **D** Fluorescence images of diploid N2 cells expressing mVenus-TOC34 grown in the photoautotrophic and heterotrophic states. Fluorescence of mVenus fused with TOC34, which visualizes the plastid envelope, and chlorophyll fluorescence of the same cells are shown. Note that the image of chlorophyll fluorescence in the heterotrophic cell was taken under stronger excitation (enhanced) than that of the photoautotrophic cell (normal). See also Supplementary Fig. 2. Scale bars = 2 μm. **E** Fluorescence images of diploid N2 cells expressing mTP-mVenus, which visualizes mitochondria, and mScarlet-PTS1, which visualizes peroxisomes, in the photoautotrophic and heterotrophic states. Fluorescence of chlorophyll, mTP-mVenus, mScarlet-PTS1, and merged images of the same cells are shown. Scale bars = 2 μm. **F** Percentage of plastid volume per cell volume, measured using 3D fluorescence images of chlorophyll in wild-type cells. Means ± SD from 20 independent cells are shown, with dots representing data points from individual cells. **G** Percentage of mitochondrial and **H** peroxisomal volumes per cell volume, measured using 3D fluorescence images of mTP-mVenus and mScarlet-PTS1, respectively. Means ± SD from 20 independent cells are shown, with dots representing data points from individual cells. **I** Transmission electron micrographs of cells (wild-type diploid N2) grown in the photoautotrophic and heterotrophic states. The images in the right column are magnified views of regions shown in the left column. n, nucleus; pt, plastid; mt, mitochondrion; v, vacuole. Scale bars = 2 μm (left) and 0.5 μm (right). Asterisks in the graphs indicate statistically significant differences based on Student's *t*-test (*$P < 0.05$; **$P < 0.01$; ***$P < 0.001$). The ratio of values in the photoautotrophic state to those in the heterotrophic state is shown above the bars.

excitation was enhanced, residual chlorophyll fluorescence could be observed even in the heterotrophic cells, which coincided with the internal region of the plastid envelope indicated by the mVenus-TOC34 fluorescence (Supplementary Fig. 2). By observing the morphology of the heterotrophic plastid through the residual chlorophyll fluorescence under enhanced excitation, it was shown that the volume of the heterotrophic plastid was about one-sixth that of the green plastid in the photoautotrophic cell (Fig. 2F). The 3D observation also showed that both the green plastid in the photoautotrophic cell and the bleached plastid in the heterotrophic cell form a single, connected organelle (Supplementary Movies 1 and 2).

To compare the morphologies of other organelles between the photoautotrophic and heterotrophic cells, we generated a *G. partita* transformant expressing both mVenus fused with a mitochondrial transit peptide (mTP-mVenus) and mScarlet fused with a peroxisome targeting signal 1 (mScarlet-PTS1) (Fig. 2E and Supplementary Movies 3 and 4). The total volume of the mitochondria in the heterotrophic cells was 1.5 times larger than that in the photoautotrophic cells (Fig. 2G), which is consistent with the elevated respiratory activity in the heterotrophic state (Fig. 1E). In both the photoautotrophic and heterotrophic cells, the peroxisomes were located adjacent to the plastid and mitochondria. The volume of peroxisomes was 1.7 times larger in the photoautotrophic cells than in the heterotrophic cells (Fig. 2H), which is likely related to the upregulation of photorespiration in the photoautotrophic cells, as shown later.

Transmission electron microscopy showed that, in the photoautotrophic cells, the plastid was filled with thylakoid membranes and phycobilisomes, which were absent in the heterotrophic plastid (Fig. 2I).

Comparison of cellular content in *G. partita* between the photoautotrophic and heterotrophic states

Despite the drastic changes in the subcellular structures (Fig. 2), the dry cell weight did not differ significantly between the photoautotrophic and heterotrophic states (Fig. 3A). The carbon content also did not differ per cell (Fig. 3B), and was only 1.1 times larger per dry cell weight in the photoautotrophic state than in the heterotrophic state (Supplementary Fig. 3A). In contrast, the nitrogen content was larger in the photoautotrophic state, 1.5 times per cell (Fig. 3C) and 1.6 times per dry cell weight (Supplementary Fig. 3B), compared to the heterotrophic state. Consistent with the higher nitrogen content, the photoautotrophic cells contained 1.3 times the amount of protein as the heterotrophic cells (Fig. 3D). SDS-polyacrylamide gel electrophoresis (PAGE) of the total cellular protein showed that proteins involved in photosynthesis, such as Rubisco (RbcL and RbcS) and phycobilisomal proteins (CpcA and CpcB), were largely reduced in the heterotrophic cells (Fig. 3E; proteins extracted from the same number of cells were separated in each lane). On the other hand, glycogen, which has been reported as the major storage glucan in *Galdieria*[51], was highly accumulated in the heterotrophic cells compared to the photoautotrophic cells, with a 17-fold difference (Fig. 3F).

The total fatty acid level was 1.7 times larger in the photoautotrophic cells than the heterotrophic cells (Fig. 3G). Analyses by thin-layer chromatography (TLC) and gas chromatography (GC) revealed that the photoautotrophic cells contained fewer phospholipids but much higher levels of glycolipids per cell (Fig. 3G, H). Levels of all glycolipids detected, namely monogalactosyldiacylglycerol (MGDG), digalactosyldiacylglycerol (DGDG), and sulfoquinovosyldiacylglycerol (SQDG), were much higher in the photoautotrophic cells (Fig. 3H). Among phospholipids, phosphatidylcholine (PC) and phosphatidylethanolamine (PE) were more abundant in the heterotrophic cells, while phosphatidylglycerol (PG) was more abundant in the photoautotrophic cells (Fig. 3H). The glycolipids (MGDG, DGDG, and SQDG) and PG are the main components of plastid envelope and thylakoid membranes[52]. Thus, the difference in the lipid composition between the photoautotrophic and heterotrophic states is largely attributable to the smaller plastid volume (Fig. 2F) and the near-complete loss of thylakoid membranes (Fig. 2I) in the heterotrophic state. Compared to the membrane lipids, triacylglycerol (TAG) content was small, with no significant difference between the photoautotrophic and heterotrophic cells (Fig. 3H).

The analysis of fatty acid composition also revealed an increase in linolenic acid (18:3), which is absent in *C. merolae*, an obligate photoautotrophic species in Cyanidiophyceae[53], along with a decrease in linoleic acid (18:2) in several lipids in the heterotrophic cells (Supplementary Fig. 3C, D). In addition, *trans*-Δ^3-hexadecenoic acid (16:1) was detected exclusively in PG in the photoautotrophic cells (Supplementary Fig. 3D), which is known to be specific to PG in plastids of land plants and algae[53,54]. Although the functions of these fatty acids are unknown in *G. partita*, they might be related to the remodeling between the photoautotrophic and heterotrophic states.

In summary, in *G. partita*, compared to the heterotrophic cell, the photoautotrophic cell contains 50% more nitrogen, 30% more proteins, and 70% more fatty acids, which are largely attributable to increases in the levels of glycolipids as major constituents of the plastid thylakoid membranes for photosynthesis (Fig. 3).

Comparison of DNA, mRNA, and rRNA levels in the nucleus/cytosol, mitochondrion, and plastid of *G. partita* in the photoautotrophic and heterotrophic states

In order to investigate how the phenotypic differences between the photoautotrophic and heterotrophic states described above are genetically achieved, DNA, mRNA, and rRNA levels in the nucleus/cytosol, mitochondrion, and plastid were compared between the two trophic states by quantitative PCR (qPCR) and RNA-seq analyses (Fig. 4).

The copy number of the plastid DNA (per nuclear DNA, determined by qPCR) was 2.2- to 2.4-fold higher in the photoautotrophic cell than in the heterotrophic cell (Fig. 4A). The plastid nucleoids, stained with SYBR Green I, were located in the center of the plastid, which is beneath the cell

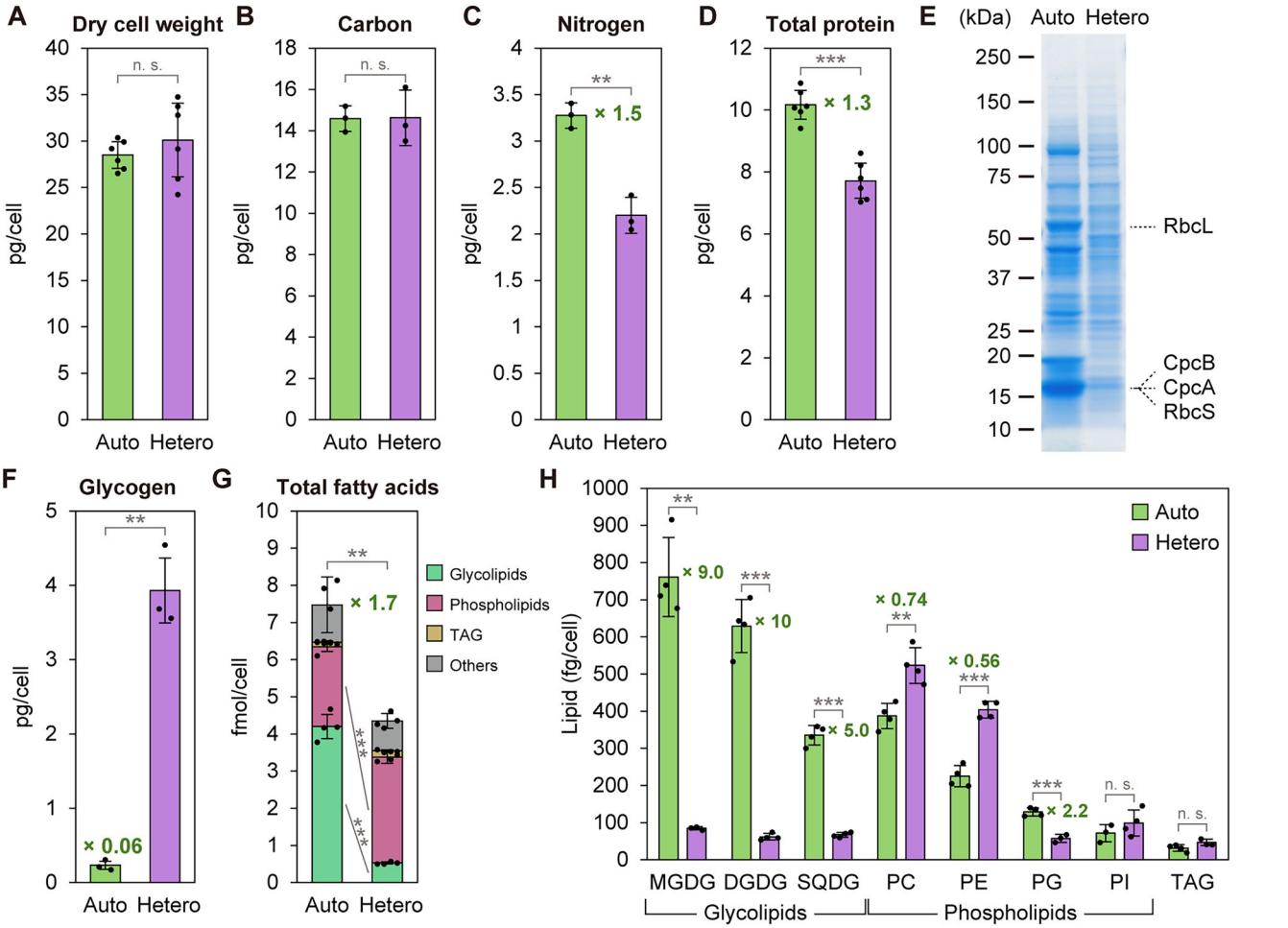

Fig. 3 | Comparison of cellular contents in *G. partita* cells between the photoautotrophic and heterotrophic states. All results are from the photoautotrophic (in the light without glucose) and heterotrophic (in the light with glucose) cultures of wild-type diploid N2. The results shown in the graphs were calculated per cell. **A** Dry cell weight. **B** Carbon content. **C** Nitrogen content. **D** Total protein content. **E** SDS-PAGE patterns of total proteins extracted from the same number of photoautotrophic and heterotrophic cells. The positions of Rubisco large subunit (RbcL), small subunit (RbcS), phycocyanin alpha subunit (CpcA), and beta subunit (CpcB) are indicated. **F** Glycogen content. **G** Total fatty acid content of all lipids extracted from the cells. **H** Membrane lipids and TAG contents. Bars represent means ± SD of results from six (**A**, **D**), three (**B**, **C**, **F**) or four (**G**, **H**) independent cultures, with dots representing individual data points. Asterisks in the graphs indicate statistically significant differences based on Student's *t*-test (*$P < 0.05$; **$P < 0.01$; ***$P < 0.001$). The ratio of values in the photoautotrophic state to those in the heterotrophic state is shown above the bars. TAG triacylglycerol, MGDG monogalactosyldiacylglycerol, DGDG digalactosyldiacylglycerol, SQDG sulfoquinovosyldiacylglycerol, PC phosphatidylcholine, PE phosphatidylethanolamine, PG phosphatidylglycerol, PI phosphatidylinositol.

membrane in the photoautotrophic cell, and were distributed along the string-shaped plastid in the heterotrophic cell (Fig. 4B). In contrast to plastid DNA, there was no significant difference in the copy number of mitochondrial DNA between the photoautotrophic and heterotrophic cells (Fig. 4A).

The rRNA copy numbers, determined by reverse transcription qPCR (RT-qPCR) and normalized per cell, showed greater differences between the photoautotrophic and heterotrophic cells compared to organelle DNA copy numbers (Fig. 4C). The photoautotrophic cell contained 4.6- to 6.2-fold more plastid rRNA, while lower levels of mitochondrial (0.31- to 0.38-fold) and cytosolic (0.59- to 0.73-fold) rRNA compared to the heterotrophic cell (Fig. 4C). These results suggest that, in the photoautotrophic cell, protein synthesis is upregulated in the plastid while downregulated in the mitochondrion and the cytosol, consistent with the above observation of the larger plastid volume accompanied by the presence of photosynthetic machinery, and the reduced mitochondrial volume, respiratory activity, and growth rate compared to the heterotrophic cell (Figs. 1 and 2).

The cytosolic and organellar mRNA levels per cell exhibited trends similar to those of rRNA when the levels were quantified by RNA-seq data, which were normalized to a spike-in control proportional to the cell number (Fig. 4D and Supplementary Data 1; see Materials and Methods). The photoautotrophic cells contained higher amounts of plastid mRNA (5.6-fold) but lower amounts of mitochondrial (0.43-fold) and cytosolic (0.54-fold) mRNA compared to the heterotrophic cells (Fig. 4D). The total (cytosolic plus organellar) mRNA levels per cell in the photoautotrophic and heterotrophic cells were similar, with only a 1.1-fold difference (Fig. 4D).

Analyses of differentially expressed genes (DEGs; a false discovery rate [FDR] < 0.01 and $|\log_2$ fold change$| > 1$) in the RNA-seq data normalized to be per cell showed that 46% of nuclear genes (3600 of 7832 protein-coding genes) were upregulated in the heterotrophic cells compared to the photoautotrophic cells (Supplementary Fig. 4A, B). However, when the RNA-seq data were normalized to the total mRNA reads in a conventional manner (i.e., without using the spike-in control), only 5.6% of nuclear genes (438 of 7832) were upregulated in the heterotrophic cells (Supplementary Fig. 4C, D). This difference in the number of DEGs between the two normalization procedures was because the overall cytosolic mRNA level of nuclear genes per cell was upregulated in the heterotrophic state.

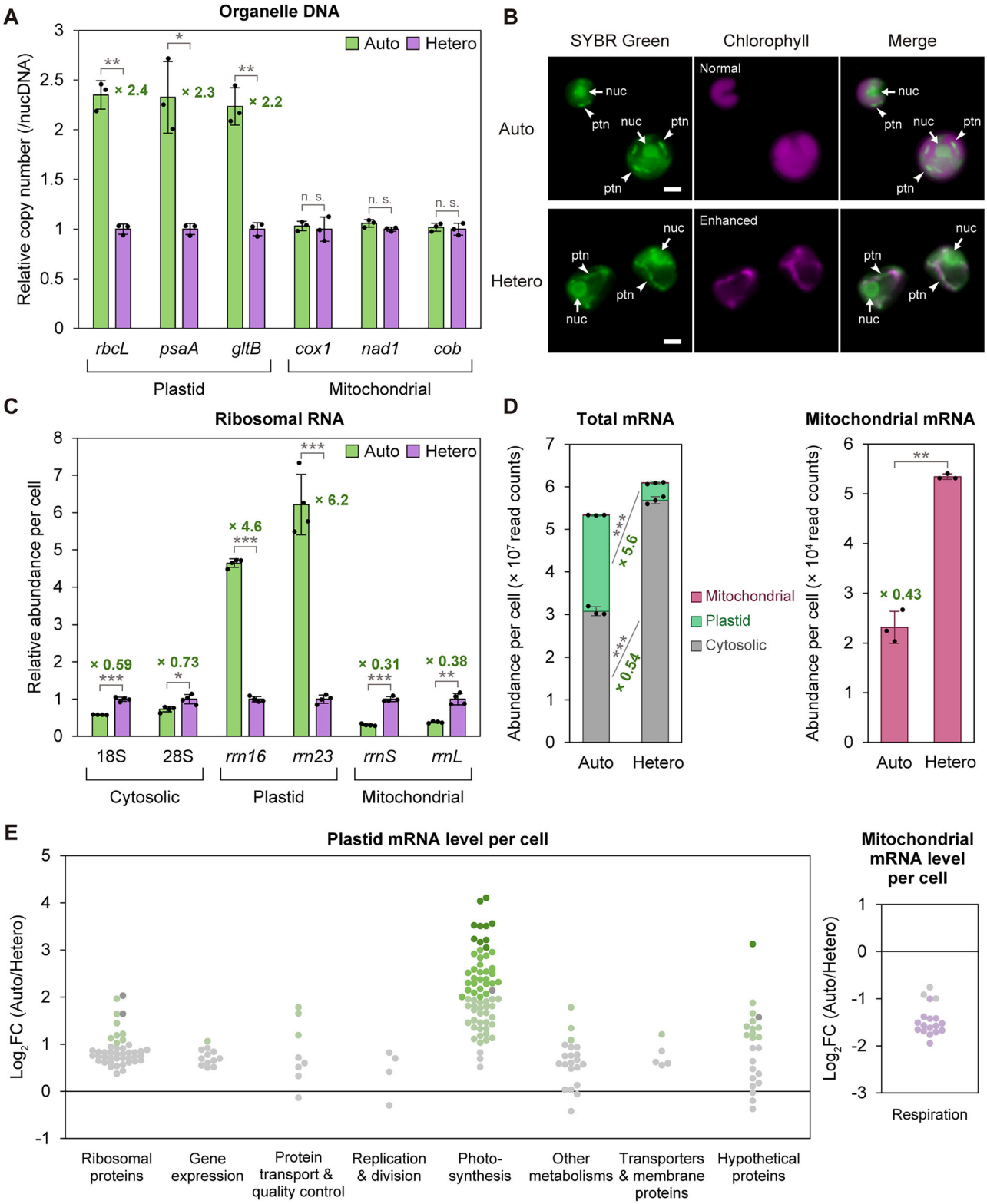

Regarding plastid mRNA levels per cell (186 protein-coding genes in total), genes involved in photosynthesis were upregulated to a larger extent than those related to other plastid functions in the photoautotrophic cells (Fig. 4E and Supplementary Fig. 5). In contrast, all of the protein-coding genes in the mitochondrial genome (18 protein-coding genes in total) encode components of the respiratory chain, and mRNA levels of most of these genes were upregulated in the heterotrophic cells (Fig. 4E and Supplementary Fig. 5).

Comparison of the proteome and metabolome of *G. partita* between the photoautotrophic and heterotrophic states

In order to further understand how cellular physiologies, including metabolisms, are remodeled between the photoautotrophic and heterotrophic states, we examined the proteome (Supplementary Data 2) and metabolome (Supplementary Data 3) for the two trophic states, also referencing the above-mentioned transcriptome (RNA-seq) data (Supplementary Data 1).

Fig. 4 | Composition of DNA, rRNA, and mRNA contents in *G. partita* cells between the photoautotrophic and heterotrophic states. All results are from the photoautotrophic (in the light without glucose) and heterotrophic (in the light with glucose) cultures of wild-type diploid N2. **A** qPCR analysis of plastid and mitochondrial DNA abundance, using primers specific to a nuclear locus (*EF1α*) as an internal control, three plastid loci (*rbcL, psaA*, and *gltB*), and three mitochondrial loci (*cox1, nad1*, and *cob*). The amount in the heterotrophic state was defined as 1.0. **B** Plastid DNA in the photoautotrophic and heterotrophic states observed by fluorescence microscopy. Fluorescence of plastid nucleoids (ptn) as well as nuclei (nuc) stained with SYBR Green I, chlorophyll fluorescence, and merged images of the same cells are shown. Note that the image of chlorophyll fluorescence in the heterotrophic cells was taken under stronger excitation (enhanced) than that of the photoautotrophic cells (normal). **C** qPCR analysis determining the relative abundance of cytosolic, plastid, and mitochondrial rRNA. Components of both large (28S, *rrn23*, and *rrnL*) and small (18S, *rrn16*, and *rrnS*) subunits are quantified. The amount in the heterotrophic state was defined as 1.0. **D** Total mRNA abundance of nuclear, plastid, and mitochondrial genome-encoded genes deduced by RNA-seq analysis. The sums of read counts normalized to be per cell are shown. **E** mRNA abundance ratio of plastid and mitochondrial genome-encoded genes between the photoautotrophic and heterotrophic cells deduced by RNA-seq analysis, shown by swarm plots. Plastid genome-encoded protein-coding genes are categorized by function, while all mitochondrial genome-encoded protein-coding genes are involved in respiration. Each dot represents a single gene, and genes with significant differences (FDR < 0.01 and $|\log_2$ fold change$| > 1$) are indicated by green or purple. See Supplementary Fig. 5 for the expression ratio of each gene. Means ± SD of results from three independent cultures are shown in (**A**, **C**, **D**), with dots representing individual data points. Asterisks in the graphs indicate statistically significant differences based on Student's *t*-test ($^*P < 0.05$; $^{**}P < 0.01$; $^{***}P < 0.001$).

G. partita nuclear, mitochondrial, and plastid genomes encode 7832, 18, and 186 proteins, respectively[41]. However, the nuclear genome contained numerous duplicated regions[41]. Thus, there are multiple pairs of proteins with identical or nearly identical amino acid sequences (many of which cannot be distinguished in proteomics), and when these are counted as the same, the number of distinct types of proteins encoded in the nuclear and organellar genomes becomes 6472, which are referred to in the proteome analysis (Supplementary Data 2; see Materials and Methods).

Of the 6472 proteins, 5147 proteins (79.5%) were detected in at least four of the six cell samples (three photoautotrophic and three heterotrophic) (Supplementary Fig. 6). The difference between the photoautotrophic and heterotrophic states in protein expression was moderately correlated with that in mRNA expression ($r = 0.69$) (Supplementary Fig. 7). In the proteome analysis, 1189 (18.4% of the total) and 656 proteins (10.1%) were expressed more than 2- and 4-fold higher in the photoautotrophic cells than in the heterotrophic cells, while 979 (15.1%) and 361 proteins (5.6%) were expressed more than 2- and 4-fold higher in the heterotrophic cells than in the photoautotrophic cells (Supplementary Fig. 6).

First, we confirmed at the protein level the results observed above in the RT-qPCR and RNA-seq analyses, namely, the levels of ribosomes in the cytoplasm, mitochondria, and plastid, as well as the expression of proteins encoded by the mitochondrial and plastid genomes. Consistent with the differences in the cytosolic, mitochondrial, and plastid rRNA and mRNA levels (Fig. 4C, D), the levels of plastid ribosomal proteins were higher in the photoautotrophic cells, while those of the cytosolic and mitochondrial ribosomal proteins were higher in the heterotrophic cells (Supplementary Fig. 8A and Supplementary Data 4). In addition, consistent with the RNA-seq results, the majority of the proteins encoded in the plastid genome were expressed more in the photoautotrophic cells than in the heterotrophic cells, while only one was more expressed in the heterotrophic cells (Supplementary Fig. 6). Some of the proteins encoded in the mitochondrial genome were more expressed in the heterotrophic cells than in the photoautotrophic state, while only one was more expressed in the photoautotrophic state (Supplementary Fig. 6). In accord with the higher expression of plastid-encoded proteins, photosynthesis-related nucleus-encoded proteins, namely all proteins constituting antenna complexes (phycobilisomes and light-harvesting complex I), photosystems, the Calvin-Benson-Bassham (Calvin) cycle, and many proteins involved in photosynthetic pigment biosynthesis, as well as photorespiration, were more expressed in the photoautotrophic cells (Supplementary Fig. 8B and Supplementary Data 5 and 6). Regarding the mitochondrion, although the levels of nucleus-encoded TCA cycle enzymes did not differ largely between the photoautotrophic and heterotrophic states, some nucleus-encoded proteins constituting the respiratory complexes were more expressed in the heterotrophic cells (Supplementary Fig. 8B and Supplementary Data 6 and 7). These differences in the protein levels in ribosomes, photosynthesis, TCA cycle, and the respiratory chain between the two trophic modes were also observed at the mRNA level (Supplementary Fig. 9).

To gain insights into which parts change and which remain unchanged between the photoautotrophic and heterotrophic states, and particularly to clarify what kinds of changes are required for photoautotrophic growth in non-plastid compartments, we classified the differentially expressed (more than 4-fold) proteins based on their deduced functions and subcellular localization (Fig. 5 and Supplementary Data 8). Based on the number of proteins for which subcellular localization could be assigned, in the photoautotrophic state, the majority of upregulated proteins were localized to the plastid (shown in green in Fig. 5), and only a small portion of the proteins localized to non-plastid compartments were upregulated (Fig. 5 and Supplementary Data 8). Most of the proteins upregulated in the photoautotrophic state were involved in protein synthesis or photosynthesis in the plastid, as expected, and a few proteins were involved in photorespiration in the peroxisome (yellow in Fig. 5). In contrast to the upregulation of proteins directly related to photosynthesis, only a limited number of non-plastid proteins involved in metabolic enzymes and solute transport (indicated by colors other than green and gray in Fig. 5) were upregulated in the photoautotrophic state (Fig. 5 and Supplementary Data 8). In contrast, in the heterotrophic state, proteins involved in protein synthesis in the cytosol (pale blue in Fig. 5) and mitochondria (red in Fig. 5), as well as respiration, were upregulated, as shown above for ribosomal levels and organelle-encoded proteins. In addition, proteins associated with cellular growth and proliferation, such as cell cycle proteins, cytoskeletal proteins, and glycosyltransferases, which are putatively involved in cell wall growth, were also upregulated, consistent with the faster growth and proliferation observed in the heterotrophic state (Fig. 5 and Supplementary Data 8).

As described above, in the photoautotrophic and heterotrophic states, the major changes in the proteome were in the balance of protein synthesis between the cytosol/mitochondrion (which is associated with cellular proliferation) and the plastid, as well as in the expression of proteins involved in photosynthesis. Because the observed additional changes, although limited, were mainly in metabolic enzymes involved in carbon metabolism (excluding photosynthetic carbon fixation), lipid metabolism, and solute transporters, we next examined these enzymes and transporters in detail.

Regarding carbon metabolism, in the glycolytic/gluconeogenic pathway (Fig. 6), notable differences in proteome between the photoautotrophic and heterotrophic states included the upregulation, in the photoautotrophic state, of an isoform of fructose-1,6-bisphosphatase (FBP3), which is involved in gluconeogenesis, as well as phosphoenolpyruvate carboxykinase (PEPCK), which converts oxaloacetate (OAA) into phosphoenolpyruvate (PEP) and CO_2, and PEP synthase (PEPS), which generates PEP from pyruvate (Fig. 6 and Supplementary Data 6). While previous studies on Cyanidiophyceae, such as *C. merolae*, an obligate photoautotrophic species, and *G. sulphuraria*, have suggested that PEPCK is involved in the C4-type CO_2-concentrating mechanism, together with phosphoenolpyruvate carboxylase (PEPC)[30,55], the increase in PEP generation in the photoautotrophic state, as also observed in the metabolome analysis (Fig. 6 and Supplementary Fig. 10), likely also contributes to enhanced lipid production as described below. In the metabolomic comparison of substrates in the glycolytic/gluconeogenic pathway, glucose 6-phosphate (G6P), fructose 6-phosphate (F6P), glyceraldehyde 3-phosphate (GAP), and pyruvate increased in the heterotrophic state, while 3-phosphoglycerate (3PGA) and PEP (as

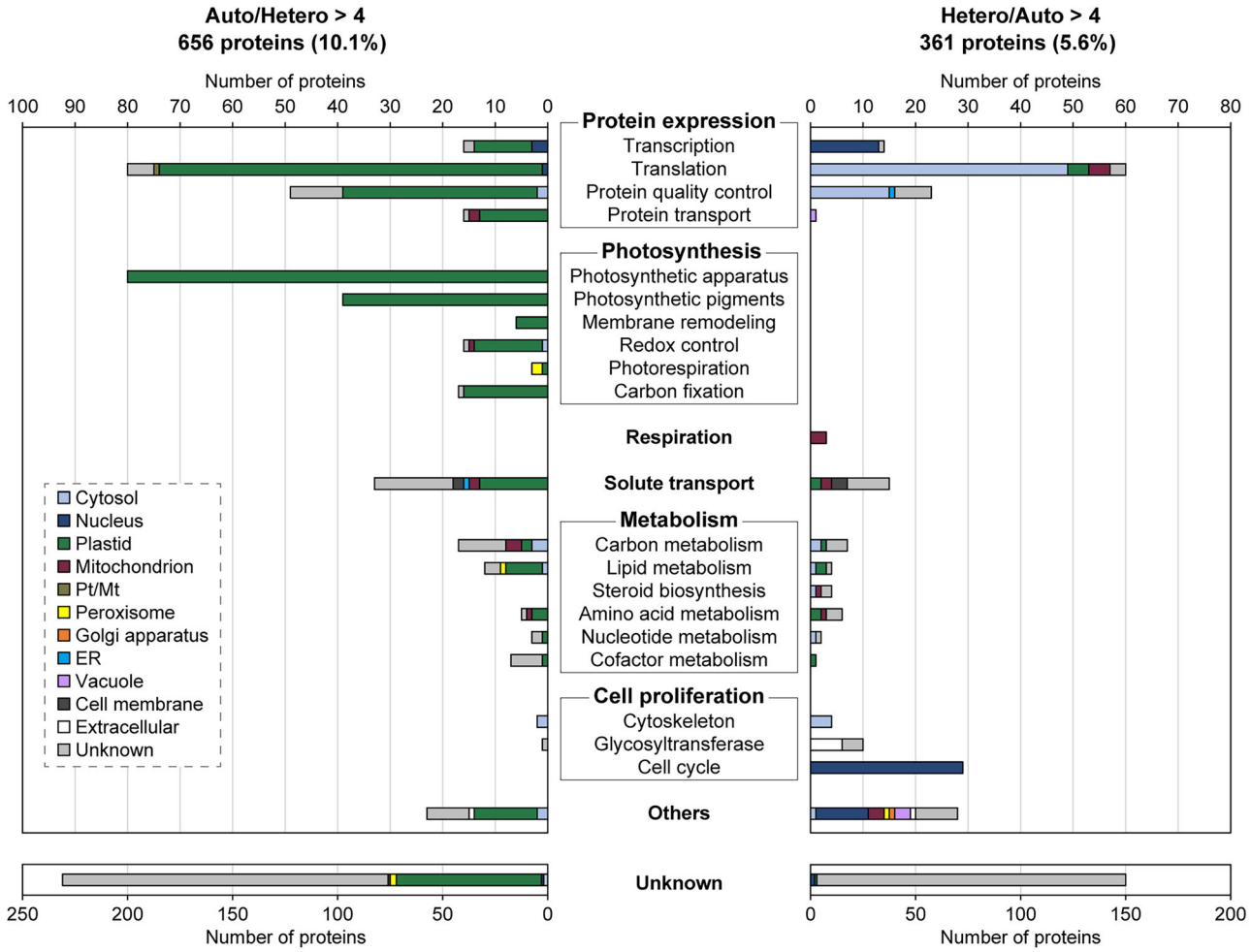

Fig. 5 | Assignments of functional categories and subcellular localizations to proteins differentially expressed between the photoautotrophic and heterotrophic states. The results are from the photoautotrophic (in the light without glucose) and heterotrophic (in the light with glucose) cultures of wild-type diploid N2. Proteins with an abundance more than 4-fold higher in the photoautotrophic (656 proteins) or heterotrophic (361 proteins) states (wild-type diploid N2), detected by DIA proteome analysis (Supplementary Fig. 6), were categorized by predicted functions, and the number of proteins in each functional category was counted. The colors indicate the deduced localization according to the color key at the lower left. The $\log_2$ fold change, deduced functional category, and localization for each protein are listed in Supplementary Data 8.

described) increased in the photoautotrophic cells (Fig. 6 and Supplementary Fig. 10). Many other metabolites, especially most sugars and sugar alcohols, were more abundant in the heterotrophic cells (Supplementary Fig. 10 and Supplementary Data 3).

In the proteomic analysis, PEP translocator (PPT), which transports PEP from the cytosol to the plastid[56], and some plastid-localized enzymes involved in fatty acid biosynthesis were upregulated in the photoautotrophic state (Fig. 6 and Supplementary Data 9 and 10). Regarding membrane lipid synthesis, MGDG synthase (MGD) and DGDG synthase (DgdA) in the plastid were upregulated in photoautotrophic cells, while the proteins involved in phospholipid biosynthesis and desaturation of fatty acids in PC were downregulated (Fig. 6 and Supplementary Data 9). These differences in the proteome of enzymes involved in lipid synthesis are consistent with those in glycolipids and phospholipids (Fig. 3G, H) and the fatty acid composition (Supplementary Fig. 3C, D) between the photoautotrophic and heterotrophic states.

Other notable differences in the lipid metabolism pathway were that several isoforms of acetyl-CoA synthetase (ACS) and long-chain acyl-CoA synthetase (ACSL) were upregulated in the photoautotrophic state (Supplementary Data 9). When fluorescent protein-tagged proteins were expressed in *G. partita*, two ACS proteins were localized to mitochondrion and one ACS protein was localized to plastid, respectively, while the ACSL proteins were localized to the cytosol and plastid, respectively (Supplementary Fig. 11). Additionally, in the photoautotrophic state, acyl-acyl carrier protein (ACP) thioesterase (AAT), which hydrolyzes acyl-ACP into fatty acids and ACP in the plastid, was downregulated, while phospholipase A2 (PLA2), which hydrolyzes PC and produces free fatty acids, was upregulated (Fig. 6). These differences suggest the possibility of alteration in the transfer of fatty acids between the plastid and endoplasmic reticulum between the two trophic states. The above-mentioned differences in the protein levels in the carbon and lipid metabolic pathways between the two trophic modes were partly similar to the differences in mRNA levels (Supplementary Fig. 12).

Regarding solute transporters, protein levels of transporters for carbon and nitrogen compounds were notably different between the photoautotrophic and heterotrophic states (Fig. 7). For example, in the photoautotrophic state, triose phosphate translocator (TPT), which was shown to localize to the plastid envelope (Fig. 7B) and transports photosynthesized triose phosphate to the cytosol, was upregulated, as well as the above-mentioned PPT, which imports PEP into the plastid for fatty acid biosynthesis (Fig. 7A).

A previous study in *G. javensis* showed that, in the heterotrophic culture compared to the photoautotrophic culture, there was down-regulation of mRNA levels of sugar-proton symporters of the major

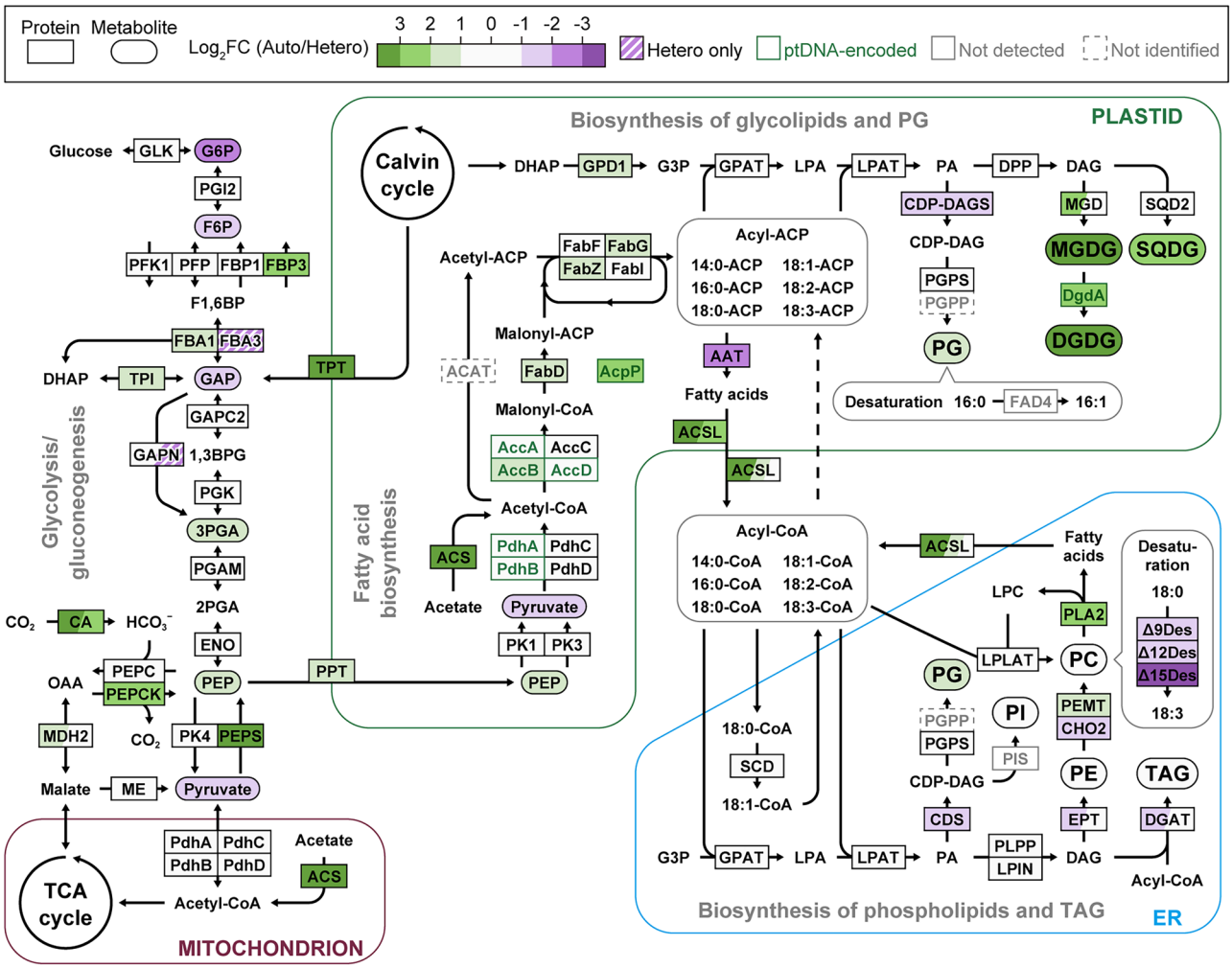

Fig. 6 | Schematic comparison of protein and metabolite abundances in the glycolytic/gluconeogenic and lipid biosynthetic pathways between the photoautotrophic and heterotrophic states. The results are from the photoautotrophic (in the light without glucose) and heterotrophic (in the light with glucose) cultures of wild-type diploid N2. The metabolic pathways, subcellular compartments (plastid, mitochondria, endoplasmic reticulum [ER], and cytosol), and abbreviated protein names are primarily based on previous studies[90,91] (see Supplementary Data 6 and 9 for detail). Square colors indicate the $\log_2$ fold change in protein abundance from DIA proteome analysis (Supplementary Data 6, 9, and 10), while rounded square colors indicate the $\log_2$-transformed metabolite ratios from GC-MS metabolome analysis (Supplementary Fig. 10; Supplementary Data 3) and lipid analysis (Fig. 3H) in wild-type diploid N2, according to the color key at the top of the figure. Metabolites that were not the targets of metabolome analysis are not surrounded by rounded squares. 'Not detected' indicates that the protein level was below the detection limit in the analysis. 'Not identified' indicates that the protein-encoding gene was not identified in the *G. partita* genome. The transport system of fatty acids from ER to plastid is largely unknown[91] (dashed arrow). 1,3BPG 1,3-bisphosphoglycerate, 2PGA 2-phosphoglycerate, 3PGA 3-phosphoglycerate, ACP acyl carrier protein, CDP-DAG CDP-diacylglycerol, DAG diacylglycerol, DGDG digalactosyldiacylglycerol, DHAP dihydroxyacetone phosphate, F1,6BP fructose 1,6-bisphosphate, F6P fructose 6-phosphate, G3P glycerol 3-phosphate, G6P glucose 6-phosphate, GAP glyceraldehyde 3-phosphate, LPA lysophosphatidic acid, LPC lysophosphatidylcholine, MGDG monogalactosyldiacylglycerol, OAA oxaloacetate, PA phosphatidic acid, PC phosphatidylcholine, PE phosphatidylethanolamine, PEP phosphoenolpyruvate, PG phosphatidylglycerol, PI phosphatidylinositol, SQDG sulfoquinovosyldiacylglycerol, TAG triacylglycerol.

facilitator superfamily (MFS), YaaH family acetate transporters, and amino acid transporters of the amino acid/auxin permease (AAAP) family[28]. In our proteome results, some of the transporters of these families were likewise downregulated in the heterotrophic state (i.e., upregulated in the photoautotrophic state); however, some of the others were upregulated in the heterotrophic state (Fig. 7A and Supplementary Data 10). Regarding the subcellular localization, two members of MFS sugar transporters that were upregulated in the photoautotrophic state localized to the cell membrane and plastid envelope, respectively (Fig. 7B). Another MFS member with an almost identical level of expression in the two trophic states localized to the plastid envelope (Fig. 7B). Another MFS member that was upregulated in the heterotrophic state localized to the cell membrane (Fig. 7B). Among the AAAP amino acid transporters, two members were upregulated in the photoautotrophic state; one localized to the plastid envelope, while the other was dually localized to the plastid envelope and cell membrane (Fig. 7). One of the three YaaH family acetate transporters localized to the cell membrane was upregulated in the photoautotrophic state, while another member was upregulated in the heterotrophic state (Fig. 7). In addition, two ammonium transporters were both upregulated in the heterotrophic state, and one of them was localized to the cell membrane (Fig. 7).

The process, mechanism, and possible triggers for bleaching and greening during the remodeling between the photoautotrophic and heterotrophic states in *G. partita*

Following the comparative analyses of the steady-state cells of the photoautotrophic and heterotrophic states described above, we next analyzed the changes in cells after adding exogenous glucose to the photoautotrophic culture in the light and after removing glucose from the heterotrophic culture in the light or dark (Fig. 8). After glucose was added to the photoautotrophic culture in the light, the cells gradually lost their color and

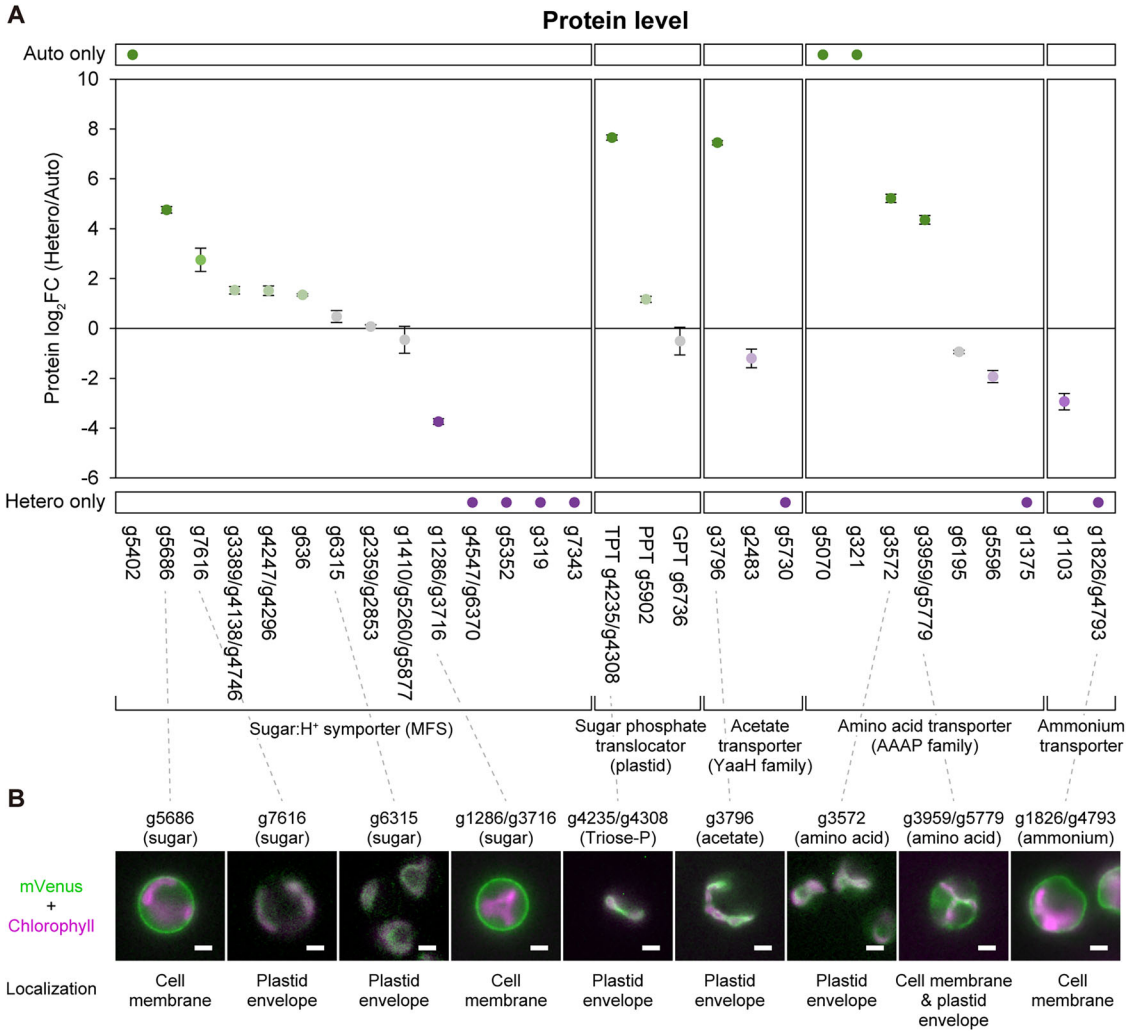

Fig. 7 | Ratios of protein abundance for sugar, sugar phosphate, acetate, amino acid, and ammonium transporters between the photoautotrophic and heterotrophic states, and the subcellular localization of some of these proteins. The proteomic results are from wild-type diploid N2 in the photoautotrophic (in the light without glucose) and heterotrophic (in the light with glucose) cultures. **A** Protein abundance ratios of sugar/H^+ symporters (MFS), sugar phosphate translocators, acetate transporters (YaaH family), amino acid transporters (AAAP family), and ammonium transporters between the photoautotrophic and heterotrophic states (Supplementary Data 10). Each dot represents a $\log_2$ fold change calculated from three independent samples per condition, with bars representing SD. Proteins detected only in the photoautotrophic samples (Auto only) or heterotrophic cell samples (Hetero only) are indicated by circles above or below the graphs, respectively. **B** Subcellular localization of representative transporter proteins. Merged images of the fluorescence of mVenus (green) and chlorophyll (magenta) are shown. The localization of each protein, as determined by observation, is shown below the images. Scale bars = 2 μm.

photosynthetic activity, becoming almost completely bleached and devoid of photosynthetic activity by 72 h (Fig. 8A and Supplementary Fig. 13C). After the glucose addition, the cells initially grew at nearly the same rate as those in the photoautotrophic state for the first 3 h but began to grow faster, resembling the steady-state heterotrophic cells, after 3 h (Fig. 8B). In addition, the respiratory activity increased sharply during the first 3 h, after which the rate of increase slowed down (Supplementary Fig. 13E). This lag of 3 h is likely required for the cells to remodel their transporter contents, as observed above in the comparison of steady-state photoautotrophic and heterotrophic cells (Fig. 7). During the bleaching process, while the chlorophyll *a* (Fig. 8C) and phycocyanin (Supplementary Fig. 13A) contents per cell gradually decreased, their contents per culture volume continued to increase, although the rate of increase relative to the growth rate was much smaller than that of photoautotrophic growth during the earlier phase of bleaching (Fig. 8D and Supplementary Fig. 13B). Thus, the bleaching process does not involve active degradation of photosynthetic pigments but solely results from their dilution due to a higher rate of cellular growth and proliferation, as well as the suppression of synthesis of photosynthetic pigment (and photosynthetic machinery as shown later).

The bleaching phenomenon has been reported in various algal species when cells are exposed to nitrogen-deficient environments, and it is considered a strategy to compensate for nitrogen deficiency by breaking down photosynthetic proteins and pigments, and other components within the cell to obtain nitrogen elements[57–59]. *G. partita* cells also bleached when they were cultured in a nitrogen-depleted inorganic medium in the light (Supplementary Fig. 14). However, unlike the case of glucose addition shown above (Fig. 8 and Supplementary Fig. 13), nitrogen depletion suppressed cellular growth and proliferation after a 4.5-fold increase in cell number, caused a gradual decrease in chlorophyll *a* content per culture volume, and led to the almost complete degradation of phycocyanin and phycobiliproteins (Supplementary Fig. 14). Thus, the bleaching caused by glucose addition to remodel the cells to the heterotrophic state is different from bleaching due to nitrogen depletion, although these two phenomena may partly share some mechanisms.

When the bleached heterotrophic cells were transferred to a glucose-free inorganic medium (glucose removal) in the light, the cells gradually turned green and eventually exhibited the same appearance (Fig. 8A) and the same levels of chlorophyll *a* (Fig. 8C) and phycocyanin (Supplementary

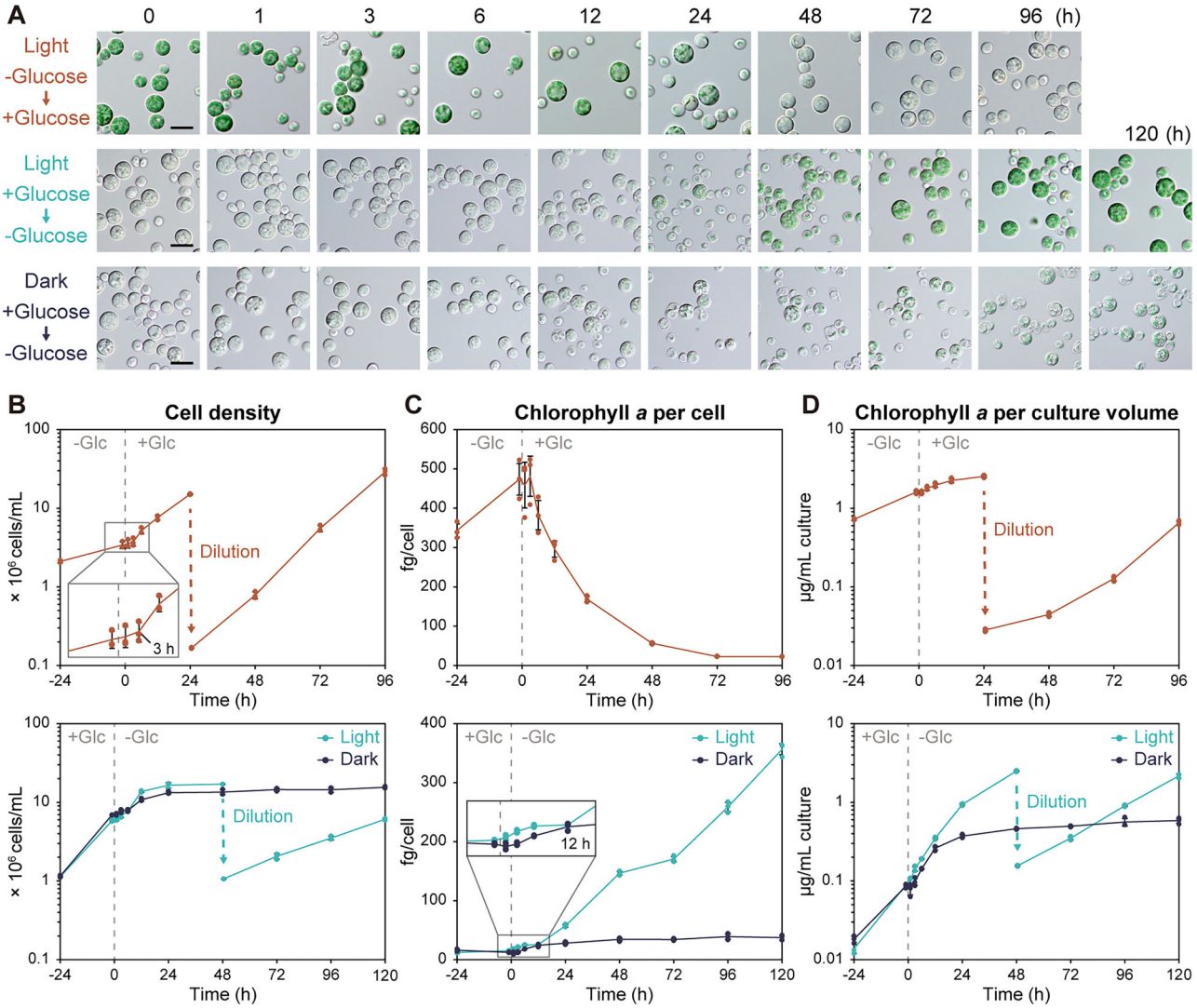

Fig. 8 | Temporal changes in *G. partita* cells following the addition and removal of exogenous glucose. In the glucose addition experiment, glucose was added to the photoautotrophic culture of wild-type diploid N2 in an inorganic medium without glucose at 0 h and cultivated in the light (red). The culture was diluted 24 h after the addition of glucose to sustain cellular growth. In the glucose removal experiment, the heterotrophic culture in a medium with glucose in the light or dark was transferred to a medium without glucose and cultivated in the light (cyan) or dark (navy). The culture in the light was diluted 48 h after the removal of glucose to sustain cellular growth. **A** Micrographs of cells captured by differential interference contrast. Scale bars = 10 µm. **B** Cell density. **C** Chlorophyll *a* content per cell. **D** Chlorophyll *a* content per culture volume. Lines and bars represent means ± SD of results from three independent cultures, with dots representing individual data points (**B–D**).

Fig. 13A) as the steady-state photoautotrophic cells 120 h after glucose removal. In addition, even in the dark, upon glucose removal, the greening of the cells also progressed until 12 h, although it ceased halfway (Fig. 8A, C), probably because external energy sources, such as light or glucose, were no longer available under this condition. These results suggest that the greening program starts upon glucose removal regardless of the availability of light (this point is later supported by the results of transcriptome analyses).

When exogenous glucose was removed, the cell number continued to increase for 24 h, and then cell proliferation almost ceased (Fig. 8B). This increase in cell number just after glucose removal occurred in both the light and the dark for the bleached cells (Fig. 8B) and, thus, was not photosynthetic growth but likely resulted from the consumption of storage materials accumulated during the heterotrophic state and/or the residual progression of cell division, or the release of daughter cells from a mother cell wall by cells that had already entered the cell division phase before glucose removal. 48 h after glucose removal, the cells resumed proliferation in the light but not in the dark (Fig. 8B). 48 h after glucose removal, the cells in the light reached a state with 40% chlorophyll *a* content (Fig. 8C) and 30% photosynthetic activity (Supplementary Fig. 13C) compared to the steady-state photoautotrophic cells. This suggests that the proliferation after 48 h was driven by photoautotrophy and that it took 48 h for the cells to transition into a state capable of photosynthetic growth. However, it took more than 96 h for the cells to be completely remodeled to the photoautotrophic state in terms of cellular chlorophyll *a* content (Fig. 8C) and photosynthetic activity (Supplementary Fig. 13C).

In order to understand the genetic basis of the cellular remodeling between the photoautotrophic and heterotrophic states, comparative transcriptomic analyses were performed on the cells during bleaching and greening at representative time points (0, 1, 6 h, and 72 or 120 h in Fig. 8) after glucose addition and removal, respectively (Supplementary Data 11; mRNA reads of nuclear genes were normalized to the total cytosolic mRNA read counts).

Principal component analysis (PCA) revealed that the transcriptomes at the beginning (0 h) of glucose addition or removal in the light were nearly identical to those at the end (72 h or 120 h) of the opposite process, respectively (Fig. 9A). This suggests that the cells were completely remodeled to the photoautotrophic or heterotrophic state by 120 h or 72 h after glucose removal or addition, respectively. However, the PCA also showed

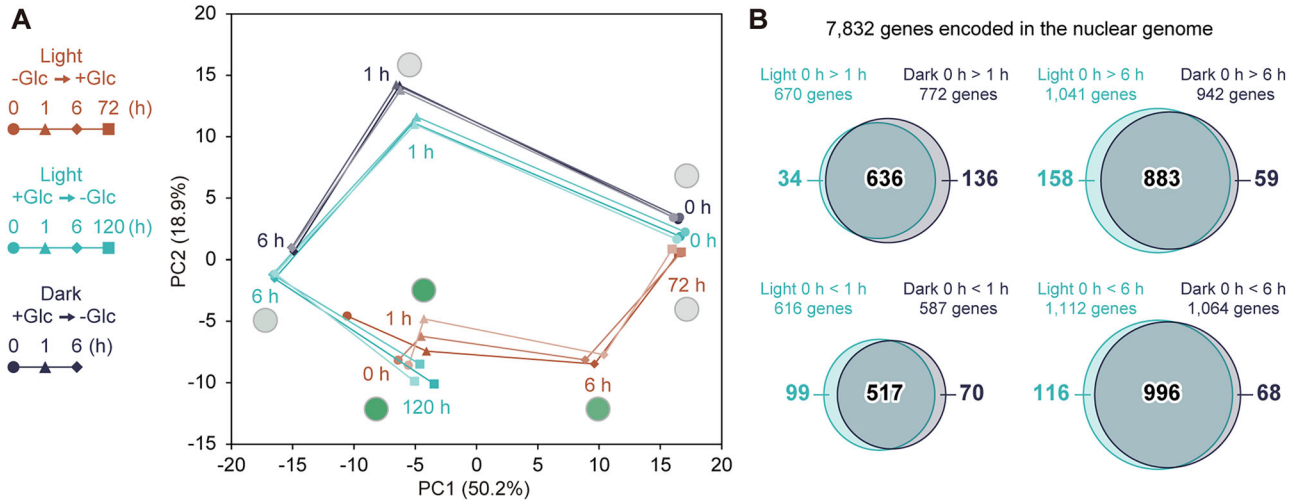

Fig. 9 | Temporal changes in the *G. partita* transcriptome following the addition and removal of exogenous glucose. The time points in each culture are the same as those in Fig. 8. The results were obtained using wild-type diploid N2. **A** A principal component analysis (PCA) of the transcriptome at representative time points based on the expression levels of all nuclear-encoded genes. The first principal component (PC1) and the second principal component (PC2) are plotted. Results from three independent cultures are shown with different color intensities. The colors of the circles indicate the approximate color of the cells at each time point. See Supplementary Fig. 15 for the PCA, including results 120 h after glucose removal in the dark. **B** Venn diagrams comparing the number of differentially expressed genes (DEGs; FDR < 0.01 and $|\log_2$ fold change$|$ > 1) between 0 h and 1 h, or 0 h and 6 h in the light and dark. The area of the circles and the overlapping regions corresponds to the number of genes.

that the processes of bleaching and greening (data at 1 and 6 h) did not follow opposite directions along the same trajectory, but instead took markedly different routes (Fig. 9A). This result is apparently reasonable because bleaching is based on accelerating cellular growth and suppressing synthesis of photosynthetic pigments and apparatus, while greening involves decelerated cellular growth and the production of photosynthetic pigments and apparatus at a pace exceeding cellular growth (Fig. 8 and Supplementary Fig. 13).

In the PCA, the cells after glucose removal in the dark, which progressed in greening similarly to those in the light until 12 h but did not continue greening thereafter (Fig. 8A, C), followed almost the same trajectory at 1 h and 6 h as the cells in the light (Fig. 9A). However, as expected, at 120 h, the cells in the dark, which had stopped greening midway, exhibited a transcriptome completely different from that of the cells in the light, which had completed greening (Supplementary Fig. 15). To address this point further, we compared the genes upregulated and downregulated at 1 h and 6 h relative to just before glucose removal (0 h) between the cells in the light and those in the dark (Fig. 9B). As a result, it was found that, both at 1 h and 6 h, almost the same sets of genes were upregulated and downregulated in both the light and the dark (Fig. 9B). These results suggest that the same greening program is triggered by glucose removal, regardless of the presence or absence of light. However, in an inorganic medium, the completion of the greening requires energy production using light as the sole external energy source.

To further understand the mechanisms of bleaching and greening, we grouped the genes that showed more than a 2-fold change in mRNA expression (3466 genes) into four clusters according to their expression patterns and performed gene ontology (GO) enrichment analysis for each cluster (Supplementary Fig. 16 and Supplementary Data 11 and 12). During the bleaching process, the genes involved in protein synthesis (cluster 3; GO terms: ribosome and translation) were gradually upregulated, while the genes involved in photosynthesis (clusters 1 and 2; GO terms: photosynthesis and thylakoid), as well as those involved in photorespiration (cluster 2; GO term: peroxisome) and redox regulation (cluster 2; GO terms: oxidoreductase activity), both of which are associated with photosynthesis, were downregulated (Supplementary Fig. 16). With regard to subcellular compartments, during the bleaching process, genes with the GO term plastid (enriched in cluster 1) were downregulated, while genes with the GO terms mitochondrion and cytosol (enriched in cluster 3) were upregulated. During the greening process, the opposite patterns were observed (Supplementary Fig. 16). These patterns aligned well with the above comparisons between the steady states of photoautotrophic and heterotrophic cells (Fig. 5). In addition, genes involved in cell proliferation (cluster 4; GO terms: cytoskeleton, DNA replication, and cell cycle) were markedly reduced at 6 h in the greening process (Supplementary Fig. 16), which is associated with the subsequent cessation of cell proliferation (Fig. 8B).

During the bleaching and greening processes, the most prominent changes were observed at 6 h in the greening process, characterized by the upregulation of photosynthesis-related genes (cluster 2 in Supplementary Fig. 16). This aligns with the necessity to synthesize photosynthesis-related proteins at a pace exceeding that of cellular growth, as observed above (Fig. 8), and is probably a reason for the difference in the trajectories of the bleaching and greening processes in the PCA of the transcriptome, as shown above (Fig. 9A).

Then, to gain insights into what activates or deactivates the bleaching and greening processes of *G. partita*, the cells were grown in media supplemented with various sugars and sugar alcohols as external organic carbon sources under both light and dark conditions (Supplementary Fig. 17). After several rounds of batch cultures to completely adapt the cells to their respective conditions, the cellular chlorophyll *a* content and the growth rate in the light and dark were determined (Supplementary Fig. 17). The cells bleached when the medium was supplemented with any sugar or sugar alcohol, both in the light and dark, but the degree of bleaching varied depending on the type of sugar or sugar alcohol (Supplementary Fig. 17). The cells were almost completely bleached with D-glucose, D-galactose, D-fructose, L-arabinose, D-xylose, D-mannose, D-sorbitol, glycerol, sucrose, and xylitol, while they retained certain levels of green color with D-mannitol, maltose, lactose, galactitol, and L-arabitol. In these cases, the cell color and chlorophyll *a* content decreased more in the dark than in the light (Supplementary Fig. 17B). Next, the extent of bleaching in respective steady state was compared with the efficiency of assimilation of each sugar or sugar alcohol, as indicated by the growth rate in the dark (Supplementary Fig. 17C). There was some correlation between the degree of bleaching and the growth rate in the dark. The growth rates in media containing D-mannitol, maltose, lactose, galactitol, and L-arabitol, where cells retained their green color, were lower than those in media with D-glucose and many

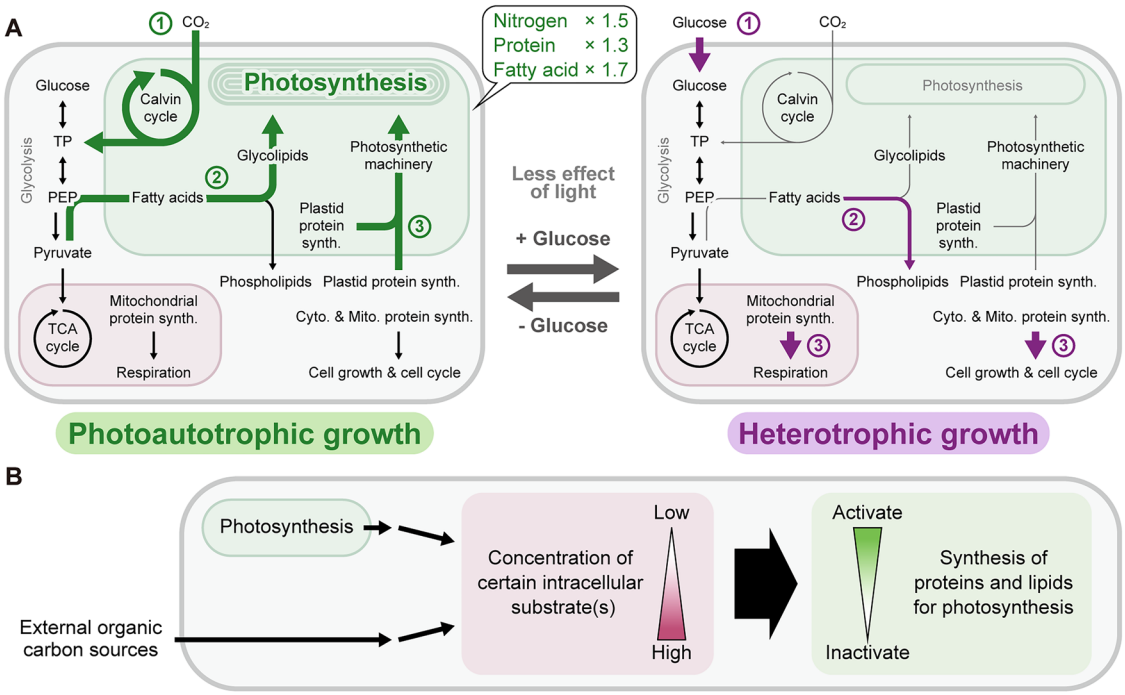

Fig. 10 | Schematic representation of the remodeling of *G. partita* cells between the photoautotrophic and heterotrophic states. A A schematic diagram comparing the photoautotrophic and heterotrophic states of *G. partita*. The photoautotrophic and heterotrophic states of *G. partita* differ mainly in (1) the source of carbohydrates (photosynthate or external organic carbon), (2) the activities of fatty acid and membrane lipid synthesis (glycolipids or phospholipids), and (3) protein synthesis activities (in the plastid or cytosol and mitochondrion). In order to enable photoautotrophic growth, the cell requires more nitrogen, protein, and fatty acids, especially glycolipids, than heterotrophic cells. When exogenous organic carbon is available, the cell ceases the synthesis of proteins and lipids required for photosynthesis, and intracellular resources are allocated more toward cell growth and proliferation. **B** The putative mechanism that triggers trophic remodeling in *G. partita* is as follows. The intracellular concentration of certain substrate(s) (e.g., a specific sugar phosphate) in sugar or carbohydrate metabolic pathways, metabolized from either organic substrate(s) obtained through photosynthesis or from outside the cell, is sensed by *G. partita* cells. Depending on the degree of the shortage of the sensed substrate(s), the cells transcribe genes encoding proteins required for photosynthesis. When the level of the sensed substrate(s) is relatively low, the cell synthesizes proteins and lipids for photosynthesis based on the degree of the shortage (greening or maintaining a steady photosynthetic state). However, when abundant exogenous organic carbon sources are available and the concentration of the substrate(s) becomes relatively high, the cell represses the synthesis of proteins and lipids for photosynthesis, while continuing to grow and proliferate, resulting in the dilution of photosynthetic machinery (bleaching or maintaining a steady heterotrophic state).

other sugars and sugar alcohols (Supplementary Fig. 17C). However, despite the very low growth rate in L-arabinose medium, the cells were almost completely bleached (Supplementary Fig. 17B, C).

Discussion

This study has highlighted three main differences between the photoautotrophic and heterotrophic states in *G. partita* (Fig. 10A and Supplementary Table 1). (1) In the photoautotrophic state, the carbon source is CO_2 fixed through photosynthesis, whereas in the heterotrophic state, the only carbon source is an external organic compound (glucose, in this study), due to the near-complete loss of photosynthetic activity. (2) The photoautotrophic cell exhibits enhanced PEP synthesis, fatty acid synthesis, and glycolipid synthesis, which are required for generating thylakoid membranes that accommodate the photosynthetic machinery in the plastid. In contrast, heterotrophic cells show greatly reduced glycolipid biosynthesis and increased phospholipid biosynthesis, supporting faster cellular growth and proliferation. (3) In the photoautotrophic state, plastid- and nucleus-encoded plastid proteins, many of which are involved in photosynthesis, are highly synthesized. In contrast, in the heterotrophic state, the synthesis of these proteins is suppressed, while cytoplasmic and mitochondrial proteins are synthesized at higher levels, supporting faster cellular growth and proliferation (Fig. 10A). Regarding the cost of photosynthesis, photoautotrophic cells require considerably more resources (1.5 times more nitrogen, 1.3 times more proteins, and 1.7 times more fatty acids per cell) compared to heterotrophic cells (Fig. 3). Meanwhile, heterotrophic cells can allocate these resources to cellular growth and grow 1.6 times faster than photoautotrophic cells (Fig. 1F). In terms of other costs, previous studies have suggested that the necessity for mechanisms to cope with reactive oxygen species generated by the photosynthetic apparatus in the light may impede the evolution of phototrophic organisms from heterotrophic ones[60]. Consistent with this idea, in *G. partita* in this study, the levels of proteins involved in redox control—such as glutathione S-transferase, thioredoxin, peroxiredoxin, and ascorbate peroxidase—were higher in the photoautotrophic state than in the heterotrophic state (Fig. 5 and Supplementary Data 8). Thus, the loss of photosynthetic machinery, even in the presence of light, would confer the benefit of reducing oxidative stress.

In the proteomics comparison of the two trophic states, changes in the enzymes involved in non-plastid metabolic pathways were relatively limited, with the levels of enzymes related to lipid synthesis varying depending on the trophic state (Figs. 5 and 6). In contrast, a greater variety of solute transporters showed changes compared to non-plastid enzymes (Figs. 5 and 7). These observations are consistent with previous physiological studies showing that, in *G. sulphuraria*, the uptake activities for respective types of sugars from the extracellular environment, rather than the activities of metabolic enzymes responsible for assimilating these compounds, change after the respective substrates are added to the medium[61].

Regarding this point, in the obligate photoautotrophic member of Cyanidiophyceae, *C. merolae*, when a plasma membrane sugar transporter, SPT1 from *G. sulphuraria*, was expressed in the cells, they became capable of heterotrophic growth in the dark with glucose, although the cells retained their green color and the growth rate was relatively low[62]. Another previous

study showed that *C. merolae* is also capable of heterotrophic growth in the dark when a very high concentration (200 mM) of glycerol is exogenously supplied[63]. In this case as well, the cells maintained their green color, and the growth rate was much lower than that of photoautotrophic growth[63]. These observations suggest that even in an obligate photoautotrophic organism, the intracellular metabolic system can support heterotrophic growth, though the efficiency is low. These observations are also apparently consistent with the results of this study in *G. partita*, where solute transporters, rather than metabolic enzymes for the assimilation of external glucose, are more modulated upon bleaching (Fig. 5). The results in *Galdieria*, where bleaching may not occur completely depending on the type of sugar or sugar alcohol provided or the algal strains[16] (Supplementary Figs. 1 and 17), and the above results in *C. merolae* both suggest that bleaching is not necessarily required for heterotrophic growth. Rather, bleaching is likely a strategy to reduce costs in natural habitats where nutrients are limited and competitors are present.

With respect to ecological contexts, the results of this study—using a homozygous diploid (*G. partita* N2) and a single organic carbon source—are useful for estimating the cost of photosynthesis, although they may reflect only one end of the range of responses observed in the organism. The degree of bleaching was highly variable, depending on the type (and likely concentration) of sugars or sugar alcohols provided (Supplementary Fig. 17), as well as among haploid clones derived from an original heterozygous diploid clone of *G. partita* (Supplementary Fig. 1). Thus, natural populations (i.e., heterozygous diploids) of *G. partita* in their native habitats probably exhibit even greater diversity in response to organic carbon availability. In contrast to *G. partita* N2 in this study, *G. sulphuraria* SAG21.92 maintained photosynthetic activity in the presence of sorbitol or glucose, though photosynthetic genes, such as those encoding components of the photosynthetic apparatus and Calvin cycle, were downregulated compared to the photoautotrophic state. In the presence of sorbitol or glucose, the cells grew mixotrophically, with a growth rate higher than under photoautotrophy or heterotrophy[30]. This study also showed that increased CO_2 supply from respiration in mixotrophy enhanced carbon fixation by photosynthesis[30]. In contrast, when external glucose was available, the green algae *A. protothecoides*[14] and *C. zofingiensis*[15] almost completely lost photosynthetic activity, even in the light, similar to *G. partita* N2 in this study. Thus, when both light and external organic carbon sources are available, mixotrophic algae seem to adopt two strategies. One strategy is the complete loss of photosynthetic activity to avoid the cost of photosynthesis, while the other is the retention of photosynthetic activity to utilize the high level of intracellular CO_2 generated by respiration, which is accelerated by the use of the taken-up organic carbon sources. Considering that both strategies are observed within Galdieriales, depending on the strain, even among clones of the same strain, as well as the type of organic compound added, it is likely that the choice of strategy depends on the specific environment to which the organism is adapted. In this regard, a recent metatranscriptomic study of Cyanidiophycean algal mats in natural environments (Yellowstone National Park) showed that, while the obligate photoautotroph *C. merolae* dominates, *Galdieria* (*G. yellowstonensis*) cells, though much less frequent—appear to be largely relegated to heterotrophy[64]. Thus, competition with other organisms likely also drives the evolution of trophic behavior[64].

The bleaching and greening processes have also been studied in the green alga *C. zofingiensis*[15], and similarities in the mechanisms are found between *C. zofingiensis* and *G. partita*. During bleaching upon glucose addition in the light, both species share common characteristics: an increase in respiratory activity, a decrease in photosynthetic activity and thylakoid membranes, accompanied by a decrease in glycolipids, as well as associated gene expression changes[15] (Fig. 8 and Supplementary Figs. 13 and 16). In addition, as observed in *G. partita* in this study, bleaching in *C. zofingiensis* is not due to the active digestion of photosynthetic pigments and machinery, which is often observed in response to nitrogen deficiency in algae[59,65] (Supplementary Fig. 14), but rather to a dilution of them caused by the suppression of their synthesis while the cells continue to grow[15] (Fig. 8). The difference between the two species lies in the destination of lipids that are no longer needed for thylakoid synthesis (glycolipids) under heterotrophic conditions. In *C. zofingiensis*, genes involved in fatty acid, TAG (triacylglycerol), and carotenoid synthesis are upregulated, leading to the accumulation of TAG and astaxanthin under heterotrophic conditions[15]. In contrast, *G. partita* redirects lipids toward cellular growth without increasing TAG or carotenoids (Fig. 3 and Supplementary Fig. 8).

Our results regarding the responses to external organic carbon sources in *G. partita* N2 showed a correlation between the efficiency of assimilation of substrates (cellular growth rate) and the extent of cell bleaching, with the exception of L-arabinose (Supplementary Fig. 17), suggesting the following hypothesis: the intracellular concentration of certain substrate(s) in sugar or carbohydrate metabolic pathways, metabolized from either photosynthates or organic substrates obtained from outside the cell, is sensed by *G. partita* cells. Depending on the degree of shortage of that substrate(s), the cells transcribe genes encoding proteins required for photosynthesis (Fig. 10B). The concentration of the metabolite(s) to be sensed would vary depending on the type of organic carbon sources available from outside the cell, due to differences in the efficiency of metabolizing the respective compound into the metabolite that is sensed. In addition, the concentration or its threshold to be sensed would vary depending on genetic polymorphisms of enzymes or the sensor(s), which may explain the difference in the degree of bleaching among strains[16] and even clones derived from the same heterozygous diploid clone (Supplementary Fig. 1). This hypothesis can also explain the higher expression of photosynthesis-related genes at the early stage of greening (6 h after glucose removal in Fig. 8 and Supplementary Fig. 16) than in the steady state of the photoautotrophic cells (120 h after glucose removal in Fig. 8 and Supplementary Fig. 16), since the substrate concentration sensed by the cells would be lower in the early stage because of limited photosynthetic activity and the unavailability of external organic carbon sources.

Regarding such a mechanism for sensing the intracellular concentration of organic carbon sources to remodel the cells and organelles, there would be, at least partly, commonalities across a broader range of eukaryotic lineages. A previous study characterizing mutants of the green alga *C. zofingiensis* showed that hexokinase is required for the repression of photosynthesis and the acceleration of TAG and carotenoid synthesis in response to the uptake of external glucose[66]. In a similar manner, in the angiosperm *Arabidopsis thaliana*, the greening of cotyledons is inhibited in seedlings when grown with exogenous glucose, and hexokinase is also required for this response[67]. In the budding yeast *Saccharomyces cerevisiae*, the number of mitochondria and respiratory activity decrease in the presence of excess glucose in the medium[68], and hexokinase is involved in glucose sensing and glucose-induced changes in gene expression[69].

Thus, the ability to remodel intracellular structures, including mitochondria and plastids with their own genomes, by sensing intracellular concentrations of organic carbon sources is widely observed in unicellular and multicellular eukaryotes. Moreover, there are some similarities in the molecular mechanisms, as described above, and in the plastid remodeling process, as observed in the green alga *C. zofingiensis* and the red alga *G. partita*. However, it remains to be clarified in future studies whether these mechanisms are derived from a common ancestor of eukaryotes or were independently acquired in each lineage. It is also unclear whether the prototype mechanism of plastid remodeling, the most complex examples of which are observed in land plants, already existed in the unicellular common ancestor of Archaeplastida or were independently developed in each lineage. Regarding this point, molecular genetic studies with genetic manipulation in *G. partita*, a member of Cyanidiophyceae that branched early in Archaeplastida evolution, will aid understanding. For example, this would include identifying hexokinase or other sensors and transcription factors, such as MYB family transcription factors g2685 and g5993, which are highly expressed in the heterotrophic state and are candidates for further analysis (Supplementary Data 8), as well as clarifying their evolutionary relationships with green algae and land plants.

Materials and methods

Algal strains and culture conditions

Galdieria partita (NBRC 102759; Biological Resource Center, National Institute of Technology and Evaluation; https://www.nite.go.jp/en/nbrc/) was used throughout this study. For genetic modification, the haploid clone N2[41], derived from the original heterozygous diploid, was used. Among the five haploid clones N1 to N5 previously isolated[41], N2 exhibited the most obvious bleaching in response to exogenous glucose (Supplementary Fig. 1). For comparison between photoautotrophic and heterotrophic cells, the homozygous diploid derived from the haploid clone N2 generated by self-diploidization (spontaneous endoreduplication) was used.

Cells of wild-type diploid N2 and its derivatives were maintained in 20 mL of MA medium[70] at pH 2.0 in 25-cm^2 tissue culture flasks (TPP Techno Plastic Products, Trasadingen, Switzerland) statically in a 2% CO_2 incubator at 42 °C with cool-white fluorescent lamps at an intensity of 50 µmol photons m^{-2} s^{-1}. The cells of wild-type haploid N2 and its derivatives were maintained in MA medium at pH 1.0, which prevents self-diploidization[41]. The pH of the medium was adjusted with sulfuric acid.

For transformation, haploid N2 cells grown in MA medium at pH 1.0 (OD_{750} = 1.5–3) were inoculated into 25 mL of MA medium supplemented with 100 mM glucose at pH 1.0 to give an OD_{750} of 0.2, in 25-cm^2 non-treated tissue culture flasks. Then, the cells were cultured on a rotary shaker (150 rpm) in a 2% CO_2 incubator at 42 °C in the light (50 µmol photons m^{-2} s^{-1}) for 2–3 days. The cells with an OD_{750} of 0.8–1.2 were used for transformation.

The culture conditions for wild-type diploid cells for comparing the photoautotrophic and heterotrophic states are listed in Supplementary Data 13. In short, the diploid cells were cultivated in MA medium at pH 2.0 (for the photoautotrophic state) or in MA medium supplemented with 100 mM glucose at pH 2.0 (for the heterotrophic state). Both cultures were placed under the same light conditions (50–80 µmol photons m^{-2} s^{-1}) or kept in the dark for some of the cultures in the heterotrophic state, as indicated, and were supplied with 2% CO_2 using a rotary shaker or aeration. Cells were cultivated for 2–3 days and collected at an OD_{750} of 0.7–1.9, when the cells were in a logarithmic growth phase in the photoautotrophic and heterotrophic states. Growth rates of the photoautotrophic and heterotrophic cells were calculated from the OD_{750} of cultures 1 and 4 days after the start of cultivation.

DNA construction and nuclear transformation

PEG-mediated transformation was performed using cell-wall-less haploid cells, which were then converted to diploids by spontaneous self-diploidization as previously described[41]. The sequences and primers used for plasmid construction and the preparation of linear DNA for transformation are listed in Supplementary Data 14. For the construction, PCR amplification, purification of PCR products, and assembly of DNA sequences were performed using KOD One PCR Master Mix (TOYOBO CO., LTD., Osaka, Japan) or PrimeSTAR Max Premix (Takara Bio Inc., Kusatsu, Japan), the QIAquick PCR Purification Kit (QIAGEN, Venlo, Netherlands), and the In-Fusion Snap Assembly Cloning Kit (Takara Bio Inc.), respectively, according to the manufacturers' instructions.

First, for other constructions, we modified the plasmid pIG1-mTP-mVenus-BSD (expressing mVenus targeted to the mitochondrion[41]; Supplementary Fig. 18A) by replacing the promoter for expressing the Blasticidin S resistance selectable marker (Blasticidin S deaminase; *BSD*) from that of *APCC* (*pAPCC*) to that of *POLYUBIQUITIN-B* (*pUBB*; the 268-bp upstream flanking sequence of the *UBB*/*GpartN1_g2033 orf*) and replacing the left arm of the chromosomal intergenic region sequence (IG1; genomic DNA sequence between *GpartN1_g7631* and *GpartN1_g7632* loci) for integrating the construct at that chromosomal site by homologous recombination, from that of haploid N1 to that of N2, generating the plasmid pGp_pE-mTP-mV_pU-BSD (Supplementary Fig. 18B) as follows. This was because *APCC* encodes a phycobilisome linker protein, whose expression ceases in the heterotrophic state, while *UBB* is expressed in both the photoautotrophic and heterotrophic states. Additionally, there is a polymorphic difference in the sequence of the left arm, but not the right arm, of IG1 between the haploid clone N1, for which the original pIG1-mTP-mVenus-BSD was generated, and N2, used in this study.

To replace the left arm of IG1 and the promoter in the original pIG1-mTP-mVenus-BSD, we amplified four DNA fragments, (1) the left arm of IG1 with the primer set Nos. 1/2 from *G. partita* N2 genomic DNA, (2) the sequence containing *ELONGATION FACTOR 1α* promoter *(pEF1α*, 500-bp of the upstream flanking sequence of *EF1α orf)*, a nucleotide sequence encoding mitochondrial transit peptide from elongation factor thermo unstable (mTP), *mVenus orf*, *β-TUBULIN* terminator (*tTUBB*, 300-bp of the downstream flanking sequence of *TUBB orf*) with primer sets Nos. 3/4 from the original plasmid, (3) *pUBB*, with the primer set Nos. 5/6 from *G. partita* N2 genomic DNA (4) DNA sequence containing *BSD orf*, *UBIQUITIN* terminator (*tUBQ*, 300-bp of the downstream flanking sequence of *UBQ orf*), the right arm of IG1, and pUC19 backbone with the primer sets Nos. 7/8 from the original plasmid. These four DNA fragments were fused using In-Fusion Snap Assembly Cloning Kit, generating the plasmid pGp_pE-mTP-mV_pU-BSD (Supplementary Fig. 18B).

To generate transformants expressing mVenus targeted into plastid envelope, the plasmid pGp_pE-ALB3-3HA-mV (expressing ALB3-mVenus) and pGp_pE-mV-3HA-TOC34 (expressing mVenus-TOC34) were generated as follows (Supplementary Fig. 18C, D). For pGp_pE-ALB3-3HA-mV, *ALBINO3 orf* (*ALB3*, *GpartN1_g3188* loci) was amplified with the primer set Nos. 9/10 from *G. partita* N2 cDNA. A nucleotide sequence encoding three repeats of HA tag (codon-optimized to *G. partita* nuclear genome; Supplementary Data 14) was commercially synthesized. The other part of plasmid was amplified with the primer set Nos. 11/12 from the plasmid pGp_pE-mTP-mV_pU-BSD as a template. These three DNA fragments were fused using In-Fusion Snap Assembly Cloning Kit. For pGp_pE-mV-3HA-TOC34, *TOC34 orf* (*GpartN1_g2517* loci) was amplified with the primer set Nos. 13/14 from *G. partita* N2 cDNA. A nucleotide sequence encoding three repeats of HA tag was amplified with the primer set Nos. 15/16. *mVenus orf* and the other part of plasmid were amplified with the primer sets Nos. 17/18 and Nos. 19/20, respectively, from the plasmid pGp_pE-mTP-mV_pU-BSD. These four DNA fragments were fused using In-Fusion Snap Assembly Cloning Kit. Though the pGp_pE-ALB3-3HA-mV was not used for investigations of the cells in this study, it was used for generating the other plasmids described later.

To generate transformants expressing mVenus targeted into mitochondria and mScarlet targeted into peroxisomes simultaneously, the plasmid pGp_mTP-mV_mS-PTS (Supplementary Fig. 18E) was prepared as follows. An *mScarlet orf* (codon-optimized to *G. partita* nuclear genome; Supplementary Data 14) was commercially synthesized and amplified with the primer set Nos. 21/22. As the primer 22 contains peroxisome targeting signal 1 (PTS1), the PCR product encodes mScarlet fused with PTS1. The promoter of *EF1α* of *Galdieria yellowstonensis* SAG108.79 (*Gy_pEF1α*; 300-bp of the upstream flanking sequence of *EF1α orf*; this was used to avoid possible recombination with *G. partita* pEF1α in the same construct) was amplified with the primer set Nos. 23/24 from *G. yellowstonensis* genomic DNA. *APCC* terminator (*tAPCC*, 300-bp downstream flanking sequence of the *APCC*/*GpartN1_g1759 orf*) was amplified with the primer set Nos. 25/26 from *G. partita* N2 genomic DNA. The *pEF1α*-mTP-*mVenus-tTUBB* cassette and the other part of plasmid were amplified with the primer sets Nos. 27/28 and Nos. 5/29, respectively, from the plasmid pGp_pE-mTP-mV_pU-BSD. These five DNA fragments were fused using In-Fusion Snap Assembly Cloning Kit.

To generate transformants expressing several isoforms of acetyl-CoA synthetase (ACS), long-chain acyl-CoA synthetase (ACSL), or transporters fused with three HA tags and mVenus, the plasmids pGp_pE-gXXXX-mV (where gXXXX corresponds to g942, g3557, g3914, g1048, g1129, g5686, g7616, g6315, g1286, g4235, g3796, g3572, g3959, and g1826) (Supplementary Fig. 18F) were prepared. The genomic region encoding each respective protein above was amplified with the primer sets Nos. 30/31 to Nos. 56/57 from *G. partita* N2 genomic DNA. The respective amplified DNA was inserted into the vector, which was amplified with the primer set

Nos. 58/59 from the plasmid pGp_pE-ALB3-3HA-mV, using the In-Fusion Snap Assembly Cloning Kit.

The linear DNA used for transformation was prepared by PCR with the primer set Nos. 60/61 (designed based on the sequence of pUC19 backbone) from the respective plasmids prepared above and purified using the QIAquick PCR Purification Kit (QIAGEN). PEG-mediated transformation of *G. partita* haploid N2 cells, as well as the selection and isolation of transformants, was performed as described previously in ref. 41. The occurrence of the recombination event in each respective transformant was confirmed by PCR using the primer set Nos. 62/63 and a cell pellet as the template. Induction and isolation of homozygous diploid cells by self-diploidization from haploid transformants were performed as described previously[41]. The diploid transformant cells were maintained in MA medium at pH 2.0.

Optical microscopy and measurement of cell and organelle sizes

The distribution of cellular volume in each respective culture was measured using Multisizer 4e (Beckman Coulter, Inc., Brea, CA, USA).

For observation of cellular morphology, the diploid cells were collected by centrifugation at 3000 × *g* for 10 min, resuspended in an appropriate volume of the supernatant (medium), and observed using a BX-51 microscope (Olympus, Tokyo, Japan) equipped with a 60× lens, Nomarski interference optics, a mercury lamp, appropriate filter sets, and DP Controller 3.2.1.276 (Olympus).

For observation of plastid morphology, diploid cells expressing mVenus-TOC34 (transformed with pGp_pE-mV-3HA-TOC34; Supplementary Fig. 18D) were used. For measurement of plastid volume per cell volume, wild-type diploid cells were used, as we confirmed that the area of chlorophyll fluorescence corresponded to that which was surrounded by mVenus-TOC34 fluorescence, indicating the plastid envelope (Fig. 2D and Supplementary Fig. 2), and was more suitable for quantification of plastid volume compared to the fluorescence of mVenus-TOC34. Chlorophyll fluorescence in the heterotrophic cells was visualized with stronger excitation than that in the photoautotrophic cells (Supplementary Fig. 2). For measurement of mitochondrial and peroxisomal volumes per cell volume and visualization of the plastids, mitochondria and peroxisomes simultaneously, diploid cells expressing mTP-mVenus and mScarlet-PTS1 (transformed with pGp_mTP-mV_mS-PTS; Supplementary Fig. 18E) was used. 300 µL of each culture was mixed with 0.1 µL of 20 mg/mL TMA-DPH (Abcam, Cambridge, United Kingdom) in DMSO on a chambered coverslip µ-Slide 8 Well (ibidi GmbH, Gräfelfing, Germany) to stain the plasma membrane. The coverslip was observed using an IX-71 inverted microscope (Olympus) equipped with a 60× lens, Nomarski interference optics, a mercury lamp, appropriate filter sets, and MetaMorph 7.10.5.476 (Molecular Devices, LLC, San Jose, CA, USA). Z-stack fluorescence photomicrographs were obtained with 0.2-µm intervals. The z-stack images were subjected to deconvolution by DeconvolutionLab2 plugin[71] and binarized on ImageJ 1.54 f (National Institutes of Health, Bethesda, MD, USA). Cell volume was measured as the volume of the space enclosed by the binarized fluorescence of TMA-DPH. Plastid volume was measured as the volume of binarized chlorophyll fluorescence of the wild-type cells. Mitochondrial and peroxisomal volumes were measured as the volume of binarized fluorescence of mTP-mVenus and that of mScarlet-PTS1, respectively.

For visualization and measurement of vacuoles, 1 mL of the wild-type diploid culture was mixed with 100 µL of Tris, pH 8.0, and 4 µL of 10 mg/mL quinacrine dihydrochloride (TCI Chemical Trading Co. Ltd., Tokyo, Japan), incubated at room temperature for 10 min, washed with MA medium at pH 2.0, and then mixed with 0.3 µL of 20 mg/mL TMA-DPH in DMSO. The cells were observed using a BX-51 microscope (Olympus) equipped with a 60× lens, Nomarski interference optics, a mercury lamp, appropriate filter sets, and controlled with DP Controller 3.2.1.276 (Olympus). As the quinacrine fluorescence rapidly decreased during excitation, z-stack images could not be obtained. Fluorescence photomicrographs of the median optical section of the cells were taken. The fluorescence images were binarized, and the area of the vacuoles stained by quinacrine and the area enclosed by the binarized fluorescence of TMA-DPH (cell area) were measured using ImageJ 1.54 f (National Institutes of Health).

For visualization of plastid nucleoids, 1 mL of the wild-type diploid culture was fixed by adding glutaraldehyde to give a final concentration of 0.35% and collected by centrifugation at 3000 × *g* for 10 min. 3 µL of resuspended cells was mixed with 0.5 µL of 1% SYBR Green I (Takara Bio Inc.) on a slide glass. The stained cells were observed using a BX-51 microscope (Olympus) equipped with a 60× lens, Nomarski interference optics, a mercury lamp, appropriate filter sets, and DP Controller 3.2.1.276 (Olympus).

For visualization of mVenus-fused ACS, ACSL and transporters, the haploid cells expressing respective proteins (g942 to g1826; Supplementary Fig. 18F) were cultivated in MA medium at pH 1.0 supplemented with 100 mM glucose and collected by centrifugation at 3000 × *g* for 10 min. The cells were observed using a BX-51 microscope (Olympus) equipped with a 60× lens, Nomarski interference optics, a mercury lamp, appropriate filter sets, and DP Controller 3.2.1.276 (Olympus).

Transmission electron microscopy

The wild-type diploid cells were collected by centrifugation at 3000 × *g* for 10 min and rapidly frozen in liquid propane at −175 °C. The frozen samples were transferred to a solution of 2% glutaraldehyde, 1% tannic acid, and 2% distilled water in acetone at −80 °C for 48 h. The samples were warmed gradually to −20 °C for 3 h, and warmed again to 4 °C for 3 h. The samples were washed with acetone at 4 °C for 10 min three times and then fixed with 2% OsO_4 in acetone at 4 °C for 2 h. The samples were then dehydrated in ethanol at room temperature for 30 min three times and then overnight, transferred to propylene oxide for 30 min twice, a 1:1 mixture of propylene oxide and Quetol-651 resin (Nisshin EM Co., Tokyo, Japan) for 3 h, and 100% Quetol-651 resin overnight. The samples were embedded in Quetol-651 resin and heated at 60°C for 48 h. Ultrathin sections (70 nm) of the samples were prepared with a diamond knife on an ultramicrotome Ultracut UCT (Leica, Vienna, Austria) and mounted on copper grids. The sections were stained with 2% uranyl acetate for 15 min and with lead stain solution (Sigma-Aldrich in Merck, Darmstadt, Germany) for 3 min at room temperature. The stained sections were then observed using an electron microscope (JEM-1400Plus; JEOL Ltd, Tokyo, Japan) with an accelerating voltage of 100 kV and a CCD camera (EM-14830RUBY2; JEOL Ltd.).

Measurement of photosynthetic and respiratory activities

Oxygen consumption and evolution rates were measured using an oxygen electrode (Oxytherm system composed of an S1/MINI Clark type electrode disc and OXYT1 electrode control unit; Hansatech, King's Lynn, United Kingdom). Two milliliters of the wild-type diploid culture were loaded into the electrode chamber at 40 °C with the culture stirred at 100 rpm. To measure oxygen consumption by respiration, the chamber was kept in the dark. To measure gross oxygen evolution, the electrode chamber was illuminated with a cool-white LED light source at an intensity of 100 µmol photons m^{-2} s^{-1}. Oxygen evolution rates by net photosynthesis were calculated by adding the oxygen consumption rates from respiration in the dark to the gross oxygen evolution rates in the light, assuming the oxygen consumption by respiration in the light is identical to that in the dark.

Quantification of cellular contents

For quantification of chlorophyll *a*, the wild-type diploid cells were collected by centrifugation at 3000 × *g* for 10 min and resuspended in 1 mL of *N*,*N*-dimethylformamide to extract chlorophyll *a*. Cells were removed by centrifugation at 15,000 × *g* for 10 min. Absorbance of the supernatant fractions at 647 and 664 nm was measured with a spectrophotometer BioSpectrometer basic (Eppendorf, Hamburg, Germany). Chlorophyll *a* content was calculated according to a previous study[72].

For quantification of dry cell weight, carbon and nitrogen content, the wild-type diploid cells were collected by centrifugation at 3000 × *g* for 10 min, washed with MA medium at pH 2.0 twice, frozen in liquid nitrogen,

and dried by a freeze dryer (FDU-1200; EYELA, Tokyo, Japan). The dry weight of the samples was measured on an electronic balance. The carbon and nitrogen contents of samples were measured using a NC analyzer (SUMIGRAPH NC-220F; Sumika Chemical Analysis Service, Ltd., Osaka, Japan).

For quantification of the total cellular protein content, the wild-type diploid cells in 10 mL of culture were collected by centrifugation at 3000 × *g* for 10 min, lysed in 1 mL of SDS sample buffer (2% [w/v] SDS, 62 mM Tris-HCl, pH 6.8, 100 mM DTT, 10% [w/v] glycerol, and 0.01% [w/v] bromophenol blue) with sonication performed 15 times for 30 s each using Bioruptor UCW-310 (Cosmo Bio, Tokyo, Japan). The protein concentration in the lysate was measured using XL-Bradford (Pharma Foods International Co., Ltd., Kyoto, Japan) according to the manufacturer's protocol.

For SDS-PAGE of total cellular protein, the wild-type diploid cells were collected by centrifugation at 3000 × *g* for 10 min, frozen in liquid nitrogen, and stored at −80 °C until use. Cells were suspended in the SDS sample buffer to give a density of 5.0×10^5 cells/μL and then sonicated 15 times for 30 s each using Bioruptor UCW-310 (Cosmo Bio). Then, the protein samples were separated on a 5–20% gradient SDS-polyacrylamide gel (ATTO Corp., Tokyo, Japan) and stained with Quick-CBB PLUS (FUJIFILM Wako Pure Chemical Corp., Osaka Japan).

Glycogen in the diploid cells was extracted based on previous methods[51,73]. The cells in 15 mL of culture were collected by centrifugation at 3000 × *g* for 10 min, frozen in liquid nitrogen, and stored at −80 °C until use. The frozen cells were resuspended in 1 mL of 90% ethanol, vortexed with glass beads (acid-washed 425−600 μm; Sigma-Aldrich in Merck) for 15 min at 4 °C to disrupt the cells, transferred to new tubes, stored at −30 °C overnight to precipitate glycogen, and harvested by centrifugation at 20,000 × *g* for 20 min. The pellets were washed with 99.5% ethanol, dissolved in 500 μL of distilled water, incubated at 98 °C for 30 min, and centrifuged at 20,000 × *g* for 5 min. The glycogen concentrations in the supernatants were measured using the EnzyChrom Glycogen Assay Kit (BioAssay Systems, Hayward, CA, USA).

Lipid analyses

The wild-type diploid cells were collected by centrifugation at 3000 × *g* for 10 min, frozen in liquid nitrogen, and stored at −80 °C until use. Total cellular lipids were extracted from the frozen cell samples according to a previous study[74]. Polar lipids were separated by two-dimensional thin-layer chromatography (TLC) on silica TLC plates (Merck) using a solvent system of chloroform/methanol/7 N ammonia water (120:80:8, v/v/v) in the first dimension, and chloroform/methanol/acetic acid/water (170:30:15:3, v/v/v/v) in the second dimension. Triacylglycerol (TAG) was separated by TLC using a solvent system of hexane/diethyl ether/acetic acid (80:20:4, v/v/v). To visualize each lipid class spot, the TLC plates were sprayed with 0.01% (w/v) primuline in 80% (v/v) acetone and then irradiated with UV light. Each lipid spot was scraped from the TLC plates, and 100 μL of 50 μg/mL pentadecanoic acid was added as an internal standard. The total lipids, without prior separation by TLC, were also mixed with the pentadecanoic acid solution. Each suspension was then incubated with 5% (v/v) HCl in methanol at 80 °C for 30 min for conversion into the corresponding fatty acid methyl esters. The methyl esters were then extracted with hexane and quantified by gas chromatography (GC-2014, Shimadzu Corp., Kyoto, Japan) equipped with a flame ionization detector and a capillary column (BPX90, 60 m × 0.25 mm; SGE Analytical Science, Milton Keynes, UK).

Quantitative PCR for quantification of organellar DNA

The wild-type diploid cells were collected by centrifugation at 3000 × *g* for 10 min and frozen in liquid nitrogen. The frozen cells were suspended in 700 μL of SDS-EB buffer (0.5% [w/v] SDS, 50 mM Tris-HCl, pH 8.0, 5 mM EDTA) and 700 μL of PCI (phenol:chloroform:isoamyl alcohol = 25:24:1) supplemented with 10 μL of PureLink RNaseA (Invitrogen in Thermo Fisher Scientific, MA, USA). The samples were then vortexed with glass beads (acid-washed 425−600 μm; Sigma-Aldrich in Merck) for 16 min at 4 °C and then centrifuged at 10,000 × *g* for 5 min. The upper aqueous phase was collected, mixed with an equal volume of PCI, briefly vortexed, and centrifuged at 10,000 × *g* for 5 min. This step was repeated twice. The upper aqueous phase was collected, mixed with an equal volume of chloroform, briefly vortexed, and centrifuged at 10,000 × *g* for 5 min. The resulting upper aqueous phase was collected, mixed with an equal volume of isopropanol and one-tenth volume of 3 M sodium acetate, vigorously inverted, and centrifuged at 15,000 × *g* for 15 min to obtain nucleic acids as pellets. The pellets were washed with 70% ethanol and dissolved in TE buffer (1 mM EDTA, 10 mM Tris-HCl, pH 8.0).

Genomic DNA from one of the photoautotrophic cell samples was serially diluted to concentrations of 10, 1, 0.1, 0.01, and 0.001 ng/μL in TE buffer to generate a standard curve. Genomic DNA from the other photoautotrophic and heterotrophic cell samples was adjusted to 1 ng/μL. For quantification of plastid and mitochondrial DNA, quantitative PCR (qPCR) was performed with CFX Duet Real-Time PCR System (Bio-Rad Laboratories, Inc., Hercules, CA, USA) in a 20 μL of reaction mixture (10 μL of Power SYBR Green Master Mix [Thermo Fisher Scientific], 0.2 μL of 50 μM forward and reverse primers, 2 μL of each genomic DNA solution, and 7.6 μL of distilled water). The DNA fragments of three plastid loci (*rbcL*, *psaA*, *gltB*), three mitochondrial loci (*cox1*, *nad1*, *cob*), and a nuclear locus (*EF1α*) were amplified with primer set Nos. 64/65 to 76/77 (Supplementary Data 14).

Reverse transcription-qPCR for quantification of rRNA and RNA-seq analysis

The wild-type diploid cells were collected by centrifugation at × *g* for 10 min, frozen in liquid nitrogen, and stored at −80 °C until use. Before RNA extraction, the cell density in each sample was measured, and *Cyanidioschyzon merolae* cells equivalent to one-tenth of the number of *G. partita* cells were added to each sample as a spike-in control. The frozen cells were suspended in 700 μL of SDS-EB buffer, and 700 μL of PCI was added to the samples. The samples were then vortexed with glass beads for 10 min at 4 °C and centrifuged at 10,000 × *g* for 5 min. Nucleic acids were purified from the upper aqueous phase through PCI and chloroform extraction, followed by isopropanol precipitation as described above, dissolved in RNase-free water, and treated with recombinant DNase I (Takara Bio Inc.) according to the manufacturer's instructions to remove genomic DNA. The resulting total RNA was then purified through PCI and chloroform extraction, followed by isopropanol precipitation as described above, and dissolved in RNase-free water.

For RT-qPCR, cDNA was synthesized from each RNA sample by PrimeScript Reverse Transcriptase (Takara Bio Inc.) according to the manufacturer's instructions. cDNA from one of the photoautotrophic cell samples was serially diluted to concentrations of 5, 0.5, 0.05, 0.005, and 0.0005 ng/μL in TE buffer to generate a standard curve. cDNA from the other photoautotrophic and heterotrophic cell samples was adjusted to 0.5 ng/μL. For quantification of cDNA from cytosolic, plastid, and mitochondrial rRNA of *G. partita* cells as well as 18S rRNA of *C. merolae* cells (as a spike-in control), qPCR was performed with CFX Duet Real-Time PCR System (Bio-Rad Laboratories, Inc.) in a 20 μL of reaction mixture (10 μL of Power SYBR Green Master Mix [Thermo Fisher Scientific], 0.2 μL of 50 μM forward and reverse primers, 2 μL of each cDNA solution, and 7.6 μL of distilled water). DNA fragments of cytosolic, plastid, and mitochondrial rRNA of both the small and large subunits of *G. partita*, and the cytosolic 18S rRNA of *C. merolae* were amplified with primer sets Nos. 78/79 to 90/91 (Supplementary Data 14).

For the RNA-seq analysis, RNA samples were subjected to library construction and ribosomal RNA removal, and then sequenced on the Illumina NovaSeq 6000 platform to obtain 150-bp paired-end reads by Novogene Co. Ltd. (Beijing, China). The sequence reads were processed by Trimmomatic 0.39[75] to remove adaptor sequences, poly A/T tails, low-quality bases, and very short reads (less than 30 bases). The processed reads were aligned to the *G. partita* and *C. merolae* genome assemblies, including the nuclear, plastid, and mitochondrial genomes[41,42] using HISAT2 version 2.2.1[76]. Mapped reads were assigned to gene models using featureCounts[77]

(part of Subread 2.0.3) with the "-fraction" option to count multi-mapping reads, as the nuclear genome of *G. partita* contains numerous duplicated regions and duplicated genes[41].

Read counts for all genes on the *G. partita* and *C. merolae* genomes were then subjected to normalization and differential expression analysis using DESeq2[78]. Two sets of size factors for normalization were calculated based on the read counts of either *C. merolae* genes (spike-in control) or *G. partita* genes, respectively. Read counts normalized with the size factors from *C. merolae* data were treated as mRNA expression levels per cell, while read counts normalized with the size factors from *G. partita* data were treated as mRNA expression levels relative to total mRNA (Supplementary Data 1). For both normalized datasets, genes with differential expression between the photoautotrophic and heterotrophic states were identified using the Wald test, with a FDR < 0.01 and $|\log_2$ fold change$| > 1$, as determined by DESeq2. Plastid- and mitochondrial-encoded genes were categorized by function according to the annotations described in a previous study[41].

Proteome analysis

The wild-type diploid cells grown in the photoautotrophic and heterotrophic conditions were collected by centrifugation at 3000 × *g* for 10 min, frozen in liquid nitrogen, and stored at −80 °C until use. The proteins were extracted from the frozen cell samples, hydrolyze to peptides, separated, and analyzed using an UltiMate 3000 RSLCnano LC system (Thermo Fisher Scientific), a Q Exactive HF-X mass spectrometer (Thermo Fisher Scientific) by Kazusa Genome Technologies Inc. (Kisarazu, Japan). The identification of peptides and quantitative analysis of obtained MS data were conducted using DIA-NN 1.8.1[79] with both precursor and protein FDRs < 0.01.

As the nuclear genome of *G. partita* contains numerous duplicated regions and duplicated genes[41], some of the proteins from duplicated genes were individually distinguished and quantified, while others were not. Therefore, proteins derived from duplicated genes (>97% identity of amino acid sequences) were treated as a single protein group, and their quantitative values were summed. Among the 6472 proteins, including nuclear, plastid, and mitochondrial genome-encoded proteins, 5627 proteins were detected in at least one of six (three photoautotrophic and three heterotrophic) samples, and 5147 proteins were detected in four or more samples. These 5147 proteins were subjected to differential expression analysis; quantitative values of the 5147 proteins were normalized by variance stabilization normalization using vsn R package[80], missing values were imputed by random forests using missForest R package[81], and differentially expressed proteins were detected by empirical Bayes method[82] with a FDR < 0.05 using limma R package and the fold change between the photoautotrophic and heterotrophic samples. Among the 480 proteins detected in three or fewer samples, proteins detected in all of the photoautotrophic or heterotrophic samples were also classified accordingly (Supplementary Fig. 6).

Assignment of predicted functions and subcellular localizations to differentially expressed genes/proteins

A provisional annotation of genes in *G. partita* was assigned using Blast2GO[83] with BLASTP search results (E-value < 1e−3) generated by DIAMOND v2.0.2.140[84] using translated amino acid sequences of all nuclear genes in *G. partita* as queries against the NCBI non-redundant database and InterProScan[85] output with ANNEX[86] and GO-slim[87] options on Blast2GO. Along with the annotation by Blast2GO, the KEGG (Kyoto Encyclopedia of Genes and Genomes) Orthology IDs were assigned to all genes in the *G. partita* genome using the KEGG Automatic Annotation Server[88]. The function and localization of the photoautotrophic- and heterotrophic-upregulated proteins (more than 4-fold) were deduced based on the annotation by Blast2GO, KEGG Orthology IDs, BLASTP search results against the *C. merolae* genome data, and the information on plastid-targeted proteins in *C. merolae*[89] and in *Arabidopsis thaliana* (The Plant Proteome Database; http://ppdb.tc.cornell.edu/) and were categorized manually. The genes encoding ribosomal proteins and transporters, as well as genes involved in photosynthesis, respiration, central carbon metabolism, and acyl lipid metabolism, were deduced based on the information described above and in previous studies in *C. merolae*[90,91].

Metabolome analysis

The wild-type diploid cells were collected by centrifugation at 3000 × *g* for 10 min, frozen in liquid nitrogen, and then dried using a freeze dryer (FDU-1200; EYELA). Hydrophilic metabolites were extracted from 5 mg of dried samples using 80% methanol, purified with MonoSpin C18 spin columns (GL Sciences Inc., Tokyo, Japan), trimethylsilylated, and analyzed using GCMS-TQ8050 NX (Shimadzu Corp.) with GCMSsolution software (Shimadzu Corp.) by Kazusa Genome Technologies Inc.

Glucose addition and removal experiments

For the glucose addition experiment, the wild-type diploid cells, precultured in MA medium at pH 2.0, were transferred to 80 mL of MA medium at pH 2.0 to achieve an OD_{750} of 0.2 in 75-cm^2 non-treated tissue culture flasks. The cells were then cultured on a rotary shaker (150 rpm) in a 2% CO_2 incubator at 42 °C, under cool-white fluorescent lamps at an intensity of 50 μmol photons m^{-2} s^{-1}. After 48 h, MA medium supplemented with 1 M glucose at pH 2.0 was added to the flask in a volume equivalent to one-ninth of the culture volume, resulting in a final glucose concentration of 100 mM. Twenty-four hours after the addition of glucose, the culture was diluted 90-fold with MA medium supplemented with 100 mM glucose at pH 2.0 in new flasks to continue logarithmic growth of the cells. Cells were collected 24 h before and immediately before the glucose addition (designated as −24 h and 0 h) and 1, 3, 6, 12, 24, 48, 72, and 96 h after the glucose addition. The collected cell samples were used for measurement of cell density by a hemocytometer, quantification of photosynthetic pigments, and measurement of photosynthetic and respiratory activities as described above. The cell samples collected immediately before the glucose addition (designated as 0 h) and 1, 6, and 72 h after the glucose addition were also subjected to the RNA-seq analysis described below.

For the glucose removal experiment, wild-type diploid cells were precultured in MA medium supplemented with 100 mM glucose at pH 2.0 for 6 days to fully transition the cells to the heterotrophic state. The cells were then transferred to 120 mL of MA medium supplemented with 100 mM glucose at pH 2.0 to achieve an OD_{750} of 0.03, in 75-cm^2 non-treated tissue culture flasks. The cells were cultured on a rotary shaker (150 rpm) in a 2% CO_2 incubator at 42 °C under cool-white fluorescent lamps at an intensity of 50 μmol photons m^{-2} s^{-1}. For the dark condition, the flasks were wrapped in aluminum foil. After 48 h, cells were collected by centrifugation, the supernatant was discarded, and cells were washed with MA medium at pH 2.0 (without glucose) and resuspended in the same volume of MA medium at pH 2.0. Forty-eight hours after glucose removal, the culture under light conditions was diluted 16-fold with MA medium at pH 2.0 in new flasks to continue logarithmic growth of the cells. Cells were collected 24 h before and immediately before glucose removal (designated as −24 h and 0 h) and at 1, 3, 6, 12, 24, 48, 72, 96, and 120 h after glucose removal. The collected cell samples were used for measuring cell density with a hemocytometer, quantifying photosynthetic pigments, and measuring photosynthetic and respiratory activities as described above. The cell samples collected immediately before glucose removal (designated as 0 h) and at 1, 6, and 120 h after glucose removal were also subjected to the RNA-seq analysis described below.

The cell samples at selected time points (0, 1, 6, and 72 h in the glucose addition experiment and 0, 1, 6, and 120 h in the glucose removal experiment) were subjected to RNA extraction as described above, except that *C. merolae* cells (used as a spike-in control) were not added to the samples. The RNA samples were subjected to strand-specific cDNA library construction and sequenced on the Illumina NovaSeq 6000 platform to obtain 150-bp paired-end reads by Novogene Co., Ltd. The sequence reads were mapped to the *G. partita* nuclear genome assembly, and read counts for all protein-encoding genes were obtained as described above. TPM (transcripts per million)[92] was calculated from the read counts to estimate transcript abundance.

A principal component analysis (PCA) was conducted using the regularized $\log_2$-transformed TPM of all nuclear genes at all the time points described above with the prcomp R function. As the transcriptome of the samples at 120 h under dark conditions in the glucose removal experiment was largely different from the others, a PCA excluding that time point was also conducted. Genes with differential expression between 0 h and 1 h, or 0 h and 6 h in the glucose removal experiment (under light and dark conditions) were detected by the Wald test with a FDR < 0.01 and $|\log_2$ fold change$|>1$ using DESeq2[78]. Moreover, genes with differential expression during the glucose addition and removal experiments under light conditions were detected by likelihood ratio test on the generalized linear model with a FDR < 0.01 using the TCC R package[93], and by more than 2-fold change between maximum and minimum gene expression (TPM) during the two experiments. Three replicate expressions of the differentially expressed genes (3466 genes) were averaged, normalized to z-scores, and subjected to k-means clustering with $k = 4$ (the number of clusters) using the kmeans R function.

GO (gene ontology) enrichment analysis was conducted using Blast2GO[83]. GO terms were assigned with BLASTP search results (E-value < 1e − 3) by DIAMOND v2.0.2.140[84] using translated amino acid sequences of all nuclear genes in *G. partita* as queries against the NCBI non-redundant database and InterProScan[85] output with ANNEX[86] and GO-slim[87] options on Blast2GO. Enrichment of GO terms in the 4 clusters by the glucose addition and removal experiments was detected by a two-sided Fisher's exact test with an odds ratio > 1 and a FDR < 0.05 as criteria.

Statistics and reproducibility

In this study, biological replicates were defined as independently cultured samples grown in separate flasks under each condition for all experiments, except for measurements of organelle size, for which biological replicates were defined as individual cells grown under each condition. The number of biological replicates for each experiment was determined to ensure that statistical analyses could be performed sufficiently. For statistical analysis, the comparison between the three conditions in Fig. 1 was performed using Tukey's honest significant difference test with R 4.4.2. The comparisons of traits between the photoautotrophic states and heterotrophic states, excluding transcriptome, proteome, and metabolome analyses, were performed using unpaired two-tailed Student's *t*-tests with R 4.4.2. In the transcriptome analysis comparing the photoautotrophic and heterotrophic states, differentially expressed genes were identified using the Wald test implemented in DESeq2. In the proteome analysis, differentially expressed proteins were identified by empirical Bayes method implemented in limma R package. In the metabolome analysis, metabolites showing significant differences were identified using unpaired two-tailed Welch's *t*-tests, followed by Benjamini-Hochberg correction for multiple comparisons with R 4.4.2. In the transcriptome analyses of glucose addition and removal experiments, differentially expressed genes were identified using the Wald test implemented in DESeq2 (for pairwise comparisons between two time points) and likelihood ratio test on the generalized linear model implemented in the TCC R package (for detecting changes across the entire experiment). In the GO enrichment analysis, a two-sided Fisher's exact test was conducted using Blast2GO.

Reporting summary

Further information on research design is available in the Nature Portfolio Reporting Summary linked to this article.

Data availability

The raw read sequence data of RNA-seq analysis have been deposited to DDBJ/EMBL/GenBank (BioProject accession number: PRJDB19545; BioSample accession numbers: SAMD00834837–SAMD00834878; DRA run accession numbers: DRR620704–DRR620745). The mass spectrometry raw data of proteome analysis has been deposited to jPOSTrepo[94] (https://repository.jpostdb.org/, ID: JPST003482, ProteomeXchange accession number: PXD058210). The sequences for all plasmids generated and used in this study are provided in GenBank format in Supplementary Data 15. The source data used to generate the graphs in the manuscript are either indicated in each figure legend or available in Supplementary Data 16. Uncropped images of SDS-PAGE gels are shown in Supplementary Fig. 19. All the other data generated in this study are included in the manuscript and supplementary data.

Received: 15 January 2025; Accepted: 23 May 2025;
Published online: 07 June 2025

References

1. Stoecker, D., Johnson, M., deVargas, C. & Not, F. Acquired phototrophy in aquatic protists. *Aquat. Microb. Ecol.* **57**, 279–310 (2009).
2. Nowack, E. C. M. & Weber, A. P. M. Genomics-informed insights into endosymbiotic organelle evolution in photosynthetic eukaryotes. *Annu. Rev. Plant Biol.* **69**, 51–84 (2018).
3. Sibbald, S. J. & Archibald, J. M. Genomic insights into plastid evolution. *Genome Biol. Evol.* **12**, 978 (2020).
4. Strassert, J. F. H., Irisarri, I., Williams, T. A. & Burki, F. A molecular timescale for eukaryote evolution with implications for the origin of red algal-derived plastids. *Nat. Commun.* **12**, 1879 (2021).
5. Flynn, K. J. et al. Misuse of the phytoplankton–zooplankton dichotomy: the need to assign organisms as mixotrophs within plankton functional types. *J. Plankton Res.* **35**, 3–11 (2013).
6. Selosse, M.-A., Charpin, M. & Not, F. Mixotrophy everywhere on land and in water: the *grand écart* hypothesis. *Ecol. Lett.* **20**, 246–263 (2017).
7. Stoecker, D. K., Hansen, P. J., Caron, D. A. & Mitra, A. Mixotrophy in the Marine Plankton. *Annu. Rev. Mar. Sci.* **9**, 311–335 (2017).
8. Kitano, M., Matsukawa, R. & Karube, I. Changes in eicosapentaenoic acid content of *Navicula saprophila*, *Rhodomonas salina* and *Nitzschia* sp. under mixotrophic conditions. *J. Appl. Phycol.* **9**, 559–563 (1997).
9. Wilken, S., Choi, C. J. & Worden, A. Z. Contrasting mixotrophic lifestyles reveal different ecological niches in two closely related marine protists. *J. Phycol.* **56**, 52–67 (2020).
10. Selosse, M.-A. & Roy, M. Green plants that feed on fungi: facts and questions about mixotrophy. *Trends Plant Sci.* **14**, 64–70 (2009).
11. Schmidt, S., Raven, J. A. & Paungfoo-Lonhienne, C. The mixotrophic nature of photosynthetic plants. *Funct. Plant Biol.* **40**, 425–438 (2013).
12. Sadali, N. M., Sowden, R. G., Ling, Q. & Jarvis, R. P. Differentiation of chromoplasts and other plastids in plants. *Plant Cell Rep.* **38**, 803–818 (2019).
13. de Vries, J., Stanton, A., Archibald, J. M. & Gould, S. B. Streptophyte terrestrialization in light of plastid evolution. *Trends Plant Sci.* **21**, 467–476 (2016).
14. Shihira-Ishikawa, I. & Hase, E. Nutritional control of cell pigmentation in *Chlorella protothecoides* with special reference to the degeneration of chloroplast induced by glucose. *Plant Cell Physiol.* **5**, 227–240 (1964).
15. Roth, M. S. et al. Regulation of oxygenic photosynthesis during trophic transitions in the green alga *Chromochloris zofingiensis*. *Plant Cell* **31**, 579–601 (2019).
16. Gross, W. & Schnarrenberger, C. Heterotrophic growth of two strains of the acido-thermophilic red alga *Galdieria sulphuraria*. *Plant Cell Physiol.* **36**, 633–638 (1995).
17. Stadnichuk, I. N. et al. Inhibition by glucose of chlorophyll a and phycocyanobilin biosynthesis in the unicellular red alga *Galdieria partita* at the stage of coproporphyrinogen III formation. *Plant Sci.* **136**, 11–23 (1998).
18. Xiao, Y. et al. Inhibition of glucose assimilation in *Auxenochlorella protothecoides* by light. *Biotechnol. Biofuels* **13**, 146 (2020).
19. Bar, E., Rise, M., Vishkautsan, M. & Arad Malis, S. Pigment and structural changes in *Chlorella zofingiensis* upon light and nitrogen stress. *J. Plant Physiol.* **146**, 527–534 (1995).

20. Chen, T. et al. Light attenuates lipid accumulation while enhancing cell proliferation and starch synthesis in the glucose-fed oleaginous microalga *Chlorella zofingiensis*. *Sci. Rep.* **5**, 14936 (2015).
21. Heifetz, P. B., Förster, B., Osmond, C. B., Giles, L. J. & Boynton, J. E. Effects of acetate on facultative autotrophy in *Chlamydomonas reinhardtii* assessed by photosynthetic measurements and stable isotope analyses. *Plant Physiol.* **122**, 1439–1445 (2000).
22. Terauchi, A. M., Peers, G., Kobayashi, M. C., Niyogi, K. K. & Merchant, S. S. Trophic status of *Chlamydomonas reinhardtii* influences the impact of iron deficiency on photosynthesis. *Photosynth. Res.* **105**, 39–49 (2010).
23. Bogaert, K. A. et al. Metabolic, physiological, and transcriptomics analysis of batch cultures of the green microalga *Chlamydomonas* grown on different acetate concentrations. *Cells* **8**, 1367 (2019).
24. Evans, J. R. Photosynthesis and nitrogen relationships in leaves of C_3 plants. *Oecologia* **78**, 9–19 (1989).
25. Makino, A. et al. Distinctive responses of ribulose-1,5-bisphosphate carboxylase and carbonic anhydrase in wheat leaves to nitrogen nutrition and their possible relationships to CO_2-transfer resistance. *Plant Physiol.* **100**, 1737–1743 (1992).
26. Raven, J. A. Comparative aspects of chrysophyte nutrition with emphasis on carbon, phosphorus and nitrogen. in *Chrysophyte Algae* (eds. Sandgren, C. D., Smol, J. P. & Kristiansen, J.) 95–118 https://doi.org/10.1017/CBO9780511752292.006 (Cambridge University Press, 1995).
27. Evans, J. R. & Clarke, V. C. The nitrogen cost of photosynthesis. *J. Exp. Bot.* **70**, 7–15 (2019).
28. Perez Saura, P., Chabi, M., Corato, A., Cardol, P. & Remacle, C. Cell adaptation of the extremophilic red microalga *Galdieria sulphuraria* to the availability of carbon sources. *Front. Plant Sci.* **13**, 978246 (2022).
29. Park, S. I. et al. Revised classification of the Cyanidiophyceae based on plastid genome data with descriptions of the Cavernulicolales ord. nov. and Galdieriales ord. nov. (Rhodophyta). *J. Phycol.* **59**, 444–466 (2023).
30. Curien, G. et al. Mixotrophic growth of the extremophile *Galdieria sulphuraria* reveals the flexibility of its carbon assimilation metabolism. *N. Phytol.* **231**, 326–338 (2021).
31. Lin, S., Offner, G. D. & Troxler, R. F. Studies on *Cyanidium caldarium* phycobiliprotein pigment mutants. *Plant Physiol.* **93**, 772–777 (1990).
32. Yoon, H. S., Müller, K. M., Sheath, R. G., Ott, F. D. & Bhattacharya, D. Defining the major lineages of red algae (Rhodophyta). *J. Phycol.* **42**, 482–492 (2006).
33. Castenholz, R. W. & McDermott, T. R. The Cyanidiales: Ecology, Biodiversity, and Biogeography. in *Red Algae in the Genomic Age* (eds. Seckbach, J. & Chapman, D. J.) vol. **13** 357–371 (Springer Netherlands, Dordrecht, 2010).
34. Rigano, C., Fuggi, A., Di Martino Rigano, V. & Aliotta, G. Studies on utilization of 2-ketoglutarate, glutamate and other amino acids by the unicellular alga *Cyanidium caldarium*. *Arch. Microbiol.* **107**, 133–138 (1976).
35. Rigano, C., Aliotta, G., Rigano, V. D., Fuggi, A. & Vona, V. Heterotrophic growth patterns in the unicellular alga *Cyanidium caldarium*. A possible role for threonine dehydrase. *Arch. Microbiol.* **113**, 191–196 (1977).
36. Barbier, G. et al. Comparative genomics of two closely related unicellular thermo-acidophilic red algae, *Galdieria sulphuraria* and *Cyanidioschyzon merolae*, reveals the molecular basis of the metabolic flexibility of *Galdieria sulphuraria* and significant differences in carbohydrate metabolism of both algae. *Plant Physiol.* **137**, 460–474 (2005).
37. Oesterhelt, C., Schmälzlin, E., Schmitt, J. M. & Lokstein, H. Regulation of photosynthesis in the unicellular acidophilic red alga *Galdieria sulphuraria*. *Plant J. Cell Mol. Biol.* **51**, 500–511 (2007).
38. Tischendorf, G. et al. Ultrastructure and enzyme complement of proplastids from heterotrophically grown cells of the red alga *Galdieria sulphuraria*. *Eur. J. Phycol.* **42**, 243–251 (2007).
39. Schönknecht, G. et al. Gene transfer from bacteria and archaea facilitated evolution of an extremophilic eukaryote. *Science* **339**, 1207–1210 (2013).
40. Rossoni, A. W. et al. The genomes of polyextremophilic cyanidiales contain 1% horizontally transferred genes with diverse adaptive functions. *eLife* **8**, e45017 (2019).
41. Hirooka, S. et al. Life cycle and functional genomics of the unicellular red alga *Galdieria* for elucidating algal and plant evolution and industrial use. *Proc. Natl. Acad. Sci. USA* **119**, e2210665119 (2022).
42. Matsuzaki, M. et al. Genome sequence of the ultrasmall unicellular red alga *Cyanidioschyzon merolae* 10D. *Nature* **428**, 653–657 (2004).
43. Qiu, H. et al. Adaptation through horizontal gene transfer in the cryptoendolithic red alga *Galdieria phlegrea*. *Curr. Biol.* **23**, R865–R866 (2013).
44. Liu, S.-L., Chiang, Y.-R., Yoon, H. S. & Fu, H.-Y. Comparative genome analysis reveals *Cyanidiococcus* gen. nov., a new extremophilic red algal genus sister to *Cyanidioschyzon* (Cyanidioschyzonaceae, Rhodophyta). *J. Phycol.* **56**, 1428–1442 (2020).
45. Cho, C. H. et al. Genome-wide signatures of adaptation to extreme environments in red algae. *Nat. Commun.* **14**, 10 (2023).
46. Ohnuma, M., Yokoyama, T., Inouye, T., Sekine, Y. & Tanaka, K. Polyethylene glycol (PEG)-mediated transient gene expression in a red alga, *Cyanidioschyzon merolae* 10D. *Plant Cell Physiol.* **49**, 117–120 (2008).
47. Fujiwara, T., Hirooka, S. & Miyagishima, S. A cotransformation system of the unicellular red alga *Cyanidioschyzon merolae* with blasticidin S deaminase and chloramphenicol acetyltransferase selectable markers. *BMC Plant Biol.* **21**, 573 (2021).
48. Yoon, H. S., Hackett, J. D., Ciniglia, C., Pinto, G. & Bhattacharya, D. A molecular timeline for the origin of photosynthetic eukaryotes. *Mol. Biol. Evol.* **21**, 809–818 (2004).
49. Bowles, A. M. C., Williamson, C. J., Williams, T. A. & Donoghue, P. C. J. Cryogenian origins of multicellularity in archaeplastida. *Genome Biol. Evol.* **16**, evae026 (2024).
50. Blouin, N. A. & Lane, C. E. Red algal parasites: models for a life history evolution that leaves photosynthesis behind again and again. *BioEssays* **34**, 226–235 (2012).
51. Shimonaga, T. et al. Variation in storage alpha-glucans of the Porphyridiales (Rhodophyta). *Plant Cell Physiol.* **49**, 103–116 (2008).
52. Block, M. A., Dorne, A. J., Joyard, J. & Douce, R. Preparation and characterization of membrane fractions enriched in outer and inner envelope membranes from spinach chloroplasts. II. Biochemical characterization. *J. Biol. Chem.* **258**, 13281–13286 (1983).
53. Sato, N. & Moriyama, T. Genomic and biochemical analysis of lipid biosynthesis in the unicellular rhodophyte *Cyanidioschyzon merolae*: lack of a plastidic desaturation pathway results in the coupled pathway of galactolipid synthesis. *Eukaryot. Cell* **6**, 1006–1017 (2007).
54. Boudière, L. et al. Glycerolipids in photosynthesis: composition, synthesis and trafficking. *Biochim. Biophys. Acta BBA - Bioenerg.* **1837**, 470–480 (2014).
55. Rademacher, N. et al. Transcriptional response of the extremophile red alga *Cyanidioschyzon merolae* to changes in CO_2 concentrations. *J. Plant Physiol.* **217**, 49–56 (2017).
56. Linka, M., Jamai, A. & Weber, A. P. M. Functional characterization of the plastidic phosphate translocator gene family from the thermo-acidophilic red alga *Galdieria sulphuraria* reveals specific adaptations of primary carbon partitioning in green plants and red algae. *Plant Physiol.* **148**, 1487–1496 (2008).
57. Sciandra, A., Lazzara, L., Claustre, H. & Babin, M. Responses of growth rate, pigment composition and optical properties of *Cryptomonas* sp. to light and nitrogen stresses. *Mar. Ecol. Prog. Ser.* **201**, 107–120 (2000).
58. Mizuta, H., Shirakura, Y. & Yasui, H. Relationship between Phycoerythrin and Nitrogen Content in *Gloiopeltis furcata* and *Porphyra yezoensis*. *Algae* **17**, 89–93 (2002).

59. Schmollinger, S. et al. Nitrogen-sparing mechanisms in *Chlamydomonas* affect the transcriptome, the proteome, and photosynthetic metabolism. *Plant Cell* **26**, 1410–1435 (2014).
60. Stephens, T. G., Gabr, A., Calatrava, V., Grossman, A. R. & Bhattacharya, D. Why is primary endosymbiosis so rare?. *N. Phytol.* **231**, 1693–1699 (2021).
61. Oesterhelt, C., Schnarrenberger, C. & Gross, W. Characterization of a sugar/polyol uptake system in the red alga *Galdieria sulphuraria*. *Eur. J. Phycol.* **34**, 271–277 (1999).
62. Fujiwara, T. et al. Integration of a *Galdieria* plasma membrane sugar transporter enables heterotrophic growth of the obligate photoautotrophic red alga *Cynanidioschyzon merolae*. *Plant Direct* **3**, e00134 (2019).
63. Moriyama, T., Mori, N. & Sato, N. Activation of oxidative carbon metabolism by nutritional enrichment by photosynthesis and exogenous organic compounds in the red alga *Cyanidioschyzon merolae*: evidence for heterotrophic growth. *SpringerPlus* **4**, 559 (2015).
64. Stephens, T. G. et al. Temporal dynamics in a red alga dominated geothermal feature in Yellowstone National Park. *ISME Commun.* **4**, ycae151 (2024).
65. Turpin, D. H. Effects of inorganic n availability on algal photosynthesis and carbon metabolism. *J. Phycol.* **27**, 14–20 (1991).
66. Roth, M. S., Westcott, D. J., Iwai, M. & Niyogi, K. K. Hexokinase is necessary for glucose-mediated photosynthesis repression and lipid accumulation in a green alga. *Commun. Biol.* **2**, 347 (2019).
67. Jang, J. C., León, P., Zhou, L. & Sheen, J. Hexokinase as a sugar sensor in higher plants. *Plant Cell* **9**, 5–19 (1997).
68. Visser, W. et al. Effects of growth conditions on mitochondrial morphology in *Saccharomyces cerevisiae*. *Antonie Van. Leeuwenhoek* **67**, 243–253 (1995).
69. Moreno, F. & Herrero, P. The hexokinase 2-dependent glucose signal transduction pathway of *Saccharomyces cerevisiae*. *FEMS Microbiol. Rev.* **26**, 83–90 (2002).
70. Minoda, A., Sakagami, R., Yagisawa, F., Kuroiwa, T. & Tanaka, K. Improvement of culture conditions and evidence for nuclear transformation by homologous recombination in a red alga, *Cyanidioschyzon merolae* 10D. *Plant Cell Physiol.* **45**, 667–671 (2004).
71. Sage, D. et al. DeconvolutionLab2: an open-source software for deconvolution microscopy. *Methods San. Diego Calif.* **115**, 28–41 (2017).
72. Wellburn, A. R. The spectral determination of chlorophylls *a* and *b*, as well as total carotenoids, using various solvents with spectrophotometers of different resolution. *J. Plant Physiol.* **144**, 307–313 (1994).
73. Sakurai, T. et al. Profiling of lipid and glycogen accumulations under different growth conditions in the sulfothermophilic red alga *Galdieria sulphuraria*. *Bioresour. Technol.* **200**, 861–866 (2016).
74. Bligh, E. G. & Dyer, W. J. A rapid method of total lipid extraction and purification. *Can. J. Biochem. Physiol.* **37**, 911–917 (1959).
75. Bolger, A. M., Lohse, M. & Usadel, B. Trimmomatic: a flexible trimmer for Illumina sequence data. *Bioinforma. Oxf. Engl.* **30**, 2114–2120 (2014).
76. Kim, D., Paggi, J. M., Park, C., Bennett, C. & Salzberg, S. L. Graph-based genome alignment and genotyping with HISAT2 and HISAT-genotype. *Nat. Biotechnol.* **37**, 907–915 (2019).
77. Liao, Y., Smyth, G. K. & Shi, W. featureCounts: an efficient general purpose program for assigning sequence reads to genomic features. *Bioinforma. Oxf. Engl.* **30**, 923–930 (2014).
78. Love, M. I., Huber, W. & Anders, S. Moderated estimation of fold change and dispersion for RNA-seq data with DESeq2. *Genome Biol.* **15**, 550 (2014).
79. Demichev, V., Messner, C. B., Vernardis, S. I., Lilley, K. S. & Ralser, M. DIA-NN: neural networks and interference correction enable deep proteome coverage in high throughput. *Nat. Methods* **17**, 41–44 (2020).
80. Huber, W., Von Heydebreck, A., Sültmann, H., Poustka, A. & Vingron, M. Variance stabilization applied to microarray data calibration and to the quantification of differential expression. *Bioinformatics* **18**, S96–S104 (2002).
81. Stekhoven, D. J. & Bühlmann, P. MissForest—non-parametric missing value imputation for mixed-type data. *Bioinformatics* **28**, 112–118 (2012).
82. Smyth, G. K. Linear models and empirical bayes methods for assessing differential expression in microarray experiments. *Stat. Appl. Genet. Mol. Biol.* **3**, Article3 (2004).
83. Conesa, A. et al. Blast2GO: a universal tool for annotation, visualization and analysis in functional genomics research. *Bioinforma. Oxf. Engl.* **21**, 3674–3676 (2005).
84. Buchfink, B., Xie, C. & Huson, D. H. Fast and sensitive protein alignment using DIAMOND. *Nat. Methods* **12**, 59–60 (2015).
85. Quevillon, E. et al. InterProScan: protein domains identifier. *Nucleic Acids Res.* **33**, W116–W120 (2005).
86. Myhre, S., Tveit, H., Mollestad, T. & Laegreid, A. Additional gene ontology structure for improved biological reasoning. *Bioinforma. Oxf. Engl.* **22**, 2020–2027 (2006).
87. Camon, E. et al. The Gene Ontology Annotation (GOA) Database: sharing knowledge in Uniprot with Gene Ontology. *Nucleic Acids Res.* **32**, D262–D266 (2004).
88. Moriya, Y., Itoh, M., Okuda, S., Yoshizawa, A. C. & Kanehisa, M. KAAS: an automatic genome annotation and pathway reconstruction server. *Nucleic Acids Res.* **35**, W182–W185 (2007).
89. Suzuki, K. & Miyagishima, S. Eukaryotic and eubacterial contributions to the establishment of plastid proteome estimated by large-scale phylogenetic analyses. *Mol. Biol. Evol.* **27**, 581–590 (2010).
90. Moriyama, T., Sakurai, K., Sekine, K. & Sato, N. Subcellular distribution of central carbohydrate metabolism pathways in the red alga *Cyanidioschyzon merolae*. *Planta* **240**, 585–598 (2014).
91. Mori, N., Moriyama, T., Toyoshima, M. & Sato, N. Construction of global acyl lipid metabolic map by comparative genomics and subcellular localization analysis in the red alga *Cyanidioschyzon merolae*. *Front. Plant Sci.* **7**, 958 (2016).
92. Wagner, G. P., Kin, K. & Lynch, V. J. Measurement of mRNA abundance using RNA-seq data: RPKM measure is inconsistent among samples. *Theory Biosci. Theor. Den. Biowissenschaften* **131**, 281–285 (2012).
93. Sun, J., Nishiyama, T., Shimizu, K. & Kadota, K. TCC: an R package for comparing tag count data with robust normalization strategies. *BMC Bioinforma.* **14**, 219 (2013).
94. Okuda, S. et al. jPOSTrepo: an international standard data repository for proteomes. *Nucleic Acids Res.* **45**, D1107–D1111 (2017).

Acknowledgements

We thank R. Tomita, R. Ujigawa, and U. Sugimoto for their technical support. This work was supported by Grant-in-Aid for Early-Career Scientists (22K15166 to S.Y.), Grant-in-Aid for JSPS Fellows (24KJ0224 to S.Y.), Grants-in-Aid for Scientific Research (24H00579 to S-y.M.) from the Japan Society for the Promotion of Science, and JST-MIRAI Program (grant no. JPMJMI22E1 to S-y.M.) from the Japan Science and Technology Agency.

Author contributions

S.Y., S.H., T.F. and S-y.M. designed research, S.Y., S.H., T.F., B.Z., F.Y., K.T., H.M., K.A. and S-y.M. performed research, S.Y., H.M. and S-y.M. analyzed data, S.Y. and S-y.M. wrote the manuscript.

Competing interests

The authors declare no competing interests.

Additional information

Supplementary information The online version contains supplementary material available at https://doi.org/10.1038/s42003-025-08284-5.

Correspondence and requests for materials should be addressed to Shota Yamashita or Shin-ya Miyagishima.

Peer review information *Communications Biology* thanks Kyle Lauersen, Kan Tanaka and the other, anonymous, reviewer(s) for their contribution to the peer review of this work. Primary Handling Editor: Tobias Goris. A peer review file is available.